The Ubiquity and Dual Nature of Ultra Compact Dwarfs

Mark A. Norris[1]⋆ & Sheila J. Kannappan[1]†

[1] *Dept. of Physics and Astronomy, University of North Carolina, Chapel Hill, CB 3255, Phillips Hall, Chapel Hill, NC 27599-3255, USA*

ABSTRACT

We present the discovery of several Ultra Compact Dwarfs (UCDs) located in field/group environments. Examination of these objects, plus literature UCDs, confirms the existence of two distinct formation channels for these compact stellar systems. We find that the UCDs we have discovered around the group elliptical NGC3923 (and most UCDs in general) have properties consistent with their being the most luminous members of the host galaxy's globular cluster (GC) system. As with GCs they are therefore likely to be the product of the most violent epochs of galaxy formation. We describe UCDs of this type as giant GCs (GGCs). In contrast, the UCD we have found associated with the isolated S0 NGC4546 is clearly the result of the stripping of a nucleated companion galaxy. The young age (∼3.4 Gyr) of the UCD, the lack of a correspondingly young GC population, the apparently short dynamical friction decay timescale (∼0.5 Gyr) of the UCD, and the presence of a counterrotating gas disc in the host galaxy (co-rotating with respect to the UCD) together suggest that this UCD is the liberated nucleus remaining after the recent stripping of a companion by NGC4546. We infer that the presence of UCDs of either category (GGC's formed in major star forming events, or stripped nuclei formed in minor mergers) can provide a useful probe of the assembly history of the host galaxy. We suggest a general scheme that unifies the formation of GCs, UCDs, and galaxy nuclei. In this picture "normal" GCs are a composite population, composed of GCs formed *in situ*, GCs acquired from accreted galaxies, and a population of lower mass stripped dwarf nuclei masquerading as GCs. Above a "scaling onset mass" of 2×10^6 M$_\odot$ (M$_V$ ∼ –10), UCDs emerge together with a mass-size relation and a likely mass-metallicity relation (the "blue tilt"). In the mass range up to 7×10^7 M$_\odot$ (M$_V$ ∼ –13) UCDs comprise a composite population of GGCs and stripped nuclei. Interestingly, dwarf nuclei have similar colours to blue GCs and UCDs across the scaling onset mass, smoothly extending the blue tilt, while nuclei of more massive galaxies and a prominent minority of UCDs extend the red locus of GCs. Above 7×10^7 M$_\odot$, UCDs must be almost exclusively stripped nuclei, as no sufficiently rich GC systems exist to populate such an extreme of the GCLF.

Key words: galaxies: individual: NGC3923, NGC4546 - galaxies: star clusters

1 INTRODUCTION

Over the past decade increasing numbers of an enigmatic class of stellar system with luminosities and sizes intermediate between globular clusters (GCs) and dwarf or compact elliptical galaxies (dEs or cEs) have been discovered. Since their discovery in the Fornax cluster (Hilker et al. 1999; Drinkwater et al. 2000) these ultra-compact dwarfs (UCDs, Phillipps et al. 2001) have been found in the cores of other galaxy clusters such as Virgo (Haşegan et al.

2005; Jones et al. 2006), Hydra I (Wehner & Harris 2007; Misgeld et al. 2008), Coma (Price et al. 2009; Madrid et al. 2010), and Centaurus (Mieske et al. 2009). More recently the first UCDs found outside of clusters have been discovered. The first confirmation was of one definite and four possible UCDs in a survey of six galaxy groups by Evstigneeva et al. (2007a), and the second was the spectroscopic confirmation by Hau et al. (2009) of a single UCD associated with the Sombrero galaxy (NGC4594/M104), which resides in a field environment. Subsequently Da Rocha et al. (2010) discovered a total of 13 UCDs in two Hickson Compact Groups.

At present the information provided by the properties

⋆ manorris@physics.unc.edu
† sheila@physics.unc.edu

of UCDs is often somewhat contradictory, leading to the consideration of three main hypotheses for the formation of UCDs:

(1) That UCDs are simply very massive "normal" GCs (e.g., Drinkwater et al. 2000; Mieske et al. 2002), formed from the collapse of individual giant molecular clouds, possibly influenced by distinct processes such as self shielding that emerge at higher mass (Murray 2009).

(2) That UCDs (plus some of what are currently considered massive GCs) are formed by the merger of young massive star clusters (YMCs) produced during the most violent epochs of galaxy formation such as during galaxy-galaxy mergers (Fellhauer & Kroupa 2002; Maraston et al. 2004). YMCs that did not undergo merging would be left to evolve into the "normal" GC population of the resulting galaxy.

(3) That UCDs are the remnant nuclei of nucleated galaxies that have been stripped of their envelopes by tidal interaction (Bekki et al. 2001; Bekki & Freeman 2003).

In both scenarios (1) and (2) the UCD hosting galaxy is expected to harbour a population of GCs with ages and abundances nearly identical to those of the UCDs with which they formed. Similarly, in both cases the luminosity function of UCDs associated with a particular galaxy should be strongly correlated with the GC luminosity function of that galaxy, irrespective of host galaxy environment. Discriminating between objects formed through route (1) or (2) will depend on the ability to predict and observe differences in the structural properties of UCDs formed by each route; we refer to both as giant globular clusters (GGCs). As both scenarios are intimately tied up with globular cluster formation, which is thought to occur mainly during the most violent periods of galaxy assembly, GGC-type UCDs can serve as tracers of the major epochs of galaxy formation.

In contrast, the third UCD formation scenario is related to minor galaxy mergers. Unlike in (1) and (2), in a stripping scenario there is no expectation of correlations between the stellar populations and luminosity functions of the UCDs and those of any GCs present. The stellar populations of UCDs formed by stripping may also display environmental dependences. Stripping should, on average, occur later in lower density environments, due to the hierarchical nature of structure formation. The nuclei of galaxies in lower density environments are also observed to display a range of ages, in contrast to the uniformly old nuclei found in the densest regions of galaxy clusters (Paudel et al. 2010a,b). This should lead to younger average ages for UCDs in lower density environments. Additionally the total number of UCDs formed by stripping is expected to be larger, and the UCDs spread more widely, in higher density environments where the tidal field is stronger (Bekki et al. 2003). These stripped-nucleus UCDs could also display significantly higher mass-to-light ratios, relative to GGC UCDs, due to the lingering presence of a dark matter component not found in GCs (Goerdt et al. 2008, although see Bekki et al. 2003 for an alternative view).

The lack of consensus that a single scenario provides a satisfactory explanation for the properties of all known UCDs has led to the suggestion that UCDs as a class consist of a "mixed bag" of objects (Hilker 2009b; Taylor et al. 2010; Da Rocha et al. 2010) formed by different routes. Only by increasing the sample size and range of parameter space probed by UCD studies can we hope to determine which formation routes are at work. One area of parameter space currently undersampled is the behaviour of UCD properties such as stellar populations, structure, and frequency as environment changes from dense cluster core to the field.

In the this paper, we analyse imaging and spectroscopy of several newly discovered UCDs associated with the group shell elliptical NGC3923 and the field S0 galaxy NGC4546, plus the known UCD near the Sombrero, a field Sa galaxy, as part of a small pilot survey of UCDs in field/group environments. We then compare to literature data to assess UCD formation scenarios. The paper is structured as follows: In Section 2 we describe the data obtained, its reduction, and analysis. In Section 3 we present our results. In Section 4 we provide a discussion of the implications of our results. In Section 5 we provide some concluding remarks.

2   OBSERVATIONS AND DATA REDUCTION

In this section we describe the data used in this study, as well as its subsequent analysis. We use archival *HST* imaging to select UCD candidates (plus comparison GCs for NGC3923) and follow-up SOAR spectroscopy to confirm the redshift association of one UCD with NGC4546, plus two UCDs with NGC3923. A third UCD candidate near NGC3923 has not been spectroscopically observed to date due to its lower luminosity. The description of the reduction of the data is straightforward, so those less interested in the finer points of the data analysis may wish to read Section 2.1 only (on the sample) before continuing to Section 3.

2.1   UCD Identification

Intrigued by the possibility that UCDs are common in all environments, we searched archival *HST* ACS or WFPC2 observations of non-cluster galaxies for UCDs. This search consisted of visually examining all *HST* ACS or WFPC2 observations of bright galaxies ($M_B < -19.0$) at a distance of 10 to 30 Mpc observable with the SOAR telescope during spring ($6 < $R.A.$ < 18$hrs, $-70 < Dec < 0$ deg), 76 galaxies in all. In total 11 UCD candidates were found (including the previously confirmed Sombrero UCD), associated with nine galaxies. Here we focus on a subset of the UCD candidates for which we have obtained spectroscopic confirmation; the remaining objects will be included in an upcoming paper examining the entire HST archive for UCDs.

UCD candidates associated with the group shell elliptical NGC3923 and the isolated S0 NGC4546 were selected for spectroscopic follow-up. These targets were selected because of the availability of ancillary data for the target galaxies: high S/N Gemini/GMOS MOS spectroscopy of NGC3923 GCs from Norris et al. (2008), and SAURON IFU spectroscopy of NGC4546 from Kuntschner et al. (2006). We also include the Sombrero UCD in the following analysis, making use of the properties derived by Hau et al. (2009).

Table 1 displays the basic properties of the galaxies under study, including the assumed extinction, distances and projected scale. Table 2 provides the log of observations, including our SOAR/Goodman imaging and spectroscopy and *HST* observations. Table 3 presents the derived photometry and recessional velocities of our UCDs. The unconfirmed UCD in the NGC3923 system is labeled "UCD3c" to indicate that it is still a candidate.

Parameter	NGC3923	NGC4546	Sombrero	Units
R.A.	11:51:01.8	12:35:29.5	12:39:59.4	h:m:s (J2000)
Dec.	-28:48:22	-03:47:35	-11:37:23	d:m:s (J2000)
V_{hel}	1739$\pm$9	1050$\pm$9	1024$\pm$5	kms^{-1}
Type	E4-5	SB(s)0-	SA(s)a	-
A_B	0.357	0.146	0.221	mag
m-M^a	31.64$\pm$0.28	30.58$\pm$0.20	29.77$\pm$0.03	mag
Distance^b	21.28$\pm$2.93	13.06$\pm$1.26	9.0$\pm$0.1	Mpc
Scale^b	103	63	44	pc/arcsec
Stellar Mass^c	1.7×10^{11}	2.7×10^{10}	8.2×10^{10}	M$_\odot$

Table 1. Properties of NGC3923, NGC4546 and the Sombrero. From NED (http://nedwww.ipac.caltech.edu) unless otherwise noted. ^{a} From Tonry et al. (2001) for NGC3923 and NGC4546 after applying -0.16 correction for recalibration of the surface brightness fluctuations distance scale by Jensen et al. (2003). The Sombrero distance is from Spitler et al. (2006). ^{b} Calculated from m-M. ^{c} Calculated as described in Section 2.7.

Galaxy	Date	Exposure Time	Seeing
NGC3923 spec*	15/04/09	8$\times$1200s	0.6$''$
NGC4546 spec*	18/04/09	6$\times$1200s	0.5$''$
NGC3923 im*	13/05/09	4$\times$60s in B,V&R	0.8$''$
NGC4546 im*	13/05/09	4$\times$60s in B,V&R	1.3$''$
Sombrero im*	13/05/09	4$\times$60s in B,V&R	1.4$''$
NGC3923 ACS†	07/12/02	1140^a, 978s^b	-
NGC4546 WFPC2$^\diamond$	16/05/94	160s^a	-
Sombrero ACS‡	08/06/03	2.7^c, 2.0^d, 1.4ks^e	-

Table 2. Log of Observations
* SOAR/GHTS † Prop ID:9399 PI:Carter
$^\diamond$ Prop ID:5446 PI:Illingworth ‡ Prop ID:9714 PI:Noll.
^{a} F606W$\sim$V. ^{b}F814W$\sim$I. ^{c}F435W$\sim$B. ^{d}F555W$\sim$V. ^{e}F625W$\sim$R.

2.2 SOAR Spectroscopy

Spectroscopic exposures of two NGC3923 UCD candidates were taken on 2009 April 15 during commissioning of the MOS mode of the Goodman High Throughput Spectrograph (GHTS, Clemens et al. 2004) on the 4.1m Southern Astrophysics Research (SOAR) Telescope. These observations comprised 8$\times$1200s exposures through 1.5$''$ wide MOS slitlets, dispersed with a 600l/mm grating, providing a spectral resolution of $\sim$6.2 Å. The proximity of the UCD candidates to NGC3923 (R$<$8 kpc) meant that the galaxy diffuse light contributed significant flux to each slitlet. Therefore, to allow the accurate "sky" subtraction of each UCD spectrum the slitlets were long ($>$17$''$). Both UCDs have spectroscopic coverage between 4520 and 7075 Å, including coverage of the Hβ, Mgb, Fe5270, and Fe5335 absorption features.

Spectroscopic observations of the NGC4546 candidate UCD were undertaken on 2009 April 18 with the Goodman spectrograph in longslit mode. The 1.68$''$ wide longslit was aligned such that the target UCD and the centre of NGC 4546 both fell on the longslit (PA: 140.7°). The object was exposed for 6$\times$1200s, again utilising the 600 l/mm grating, this time providing a spectral resolution of $\sim$6.3 Å and a wavelength coverage of 4350 $-$ 7000 Å.

Standard IRAF routines were used to carry out bias subtraction, flatfielding, and wavelength calibration. Spectra from individual exposures were traced and extracted using APALL. Because of the relatively large regions available for sky estimation and the varying contribution of host galaxy
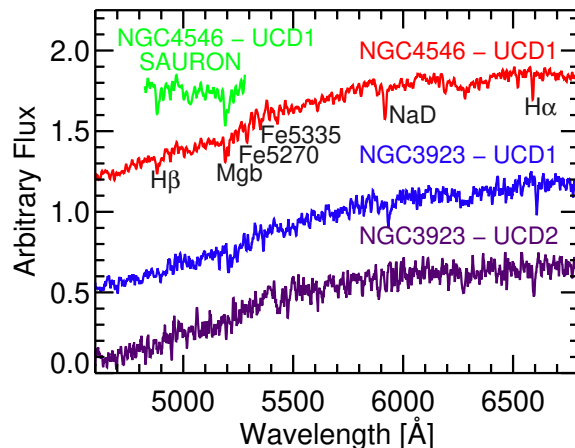

Figure 1. SOAR/Goodman UCD spectra plus SAURON continuum-normalised spectrum of NGC4546 UCD1 (full coverage shown). Redshifted absorption lines are apparent.

diffuse light across the slit/slitlets, the background "sky" across each spectral column was fitted with a low order polynomial and subtracted. The extractions were unweighted as the use of variance weighting was inadvisable due to the slightly resolved nature of these objects. Individual extracted spectra were combined using the task SCOMBINE.

The final UCD spectra are displayed in Figure 1. Redshifted absorption lines are obvious in NGC4546-UCD1 and NGC3923-UCD1, and the resulting spectra are of sufficient S/N to measure absorption line velocities in all cases. However, due to a since rectified problem with stray light sources within the instrument, the spectra are not suitable for the study of the stellar populations of the UCDs. It proved impossible to adequately remove the stray light signal during processing, leading to compromised line strength estimates.

Recessional velocities were measured using the IRAF Fourier cross correlation code FXCOR. We made use of MILES simple stellar population models (Vazdekis et al. 2010) as velocity templates, using 24 SSPs spanning the age range 1.8 to 12.6 Gyr and the metallicity range [M/H] $= -1.68$ to $+0.2$, to minimise the effects of template mismatch. The quoted velocity in Table 3 is the 3σ clipped mean of the 24 determined velocities (one per template), quoting the median error for the unclipped velocities.
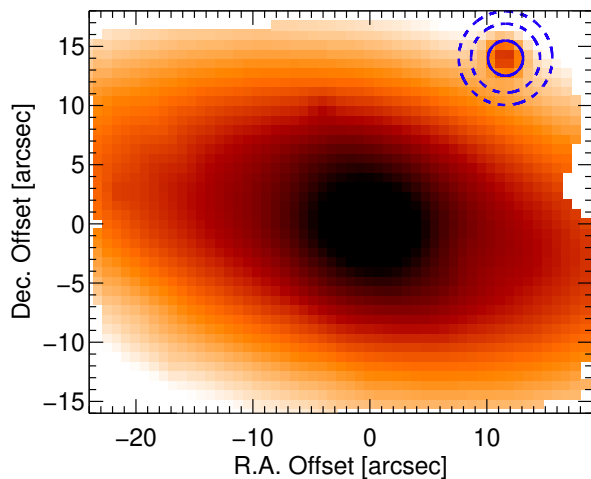
Figure 2. Log(Flux) in the SAURON NGC4546 datacube. The UCD is obvious in the top right. The solid blue circle shows the radius within which the lenslets are coadded to produce the UCD spectrum. The dashed blue circles denote the annulus within which lenslets are coadded to produce an estimate of the sky + NGC4546 diffuse light background.

2.3 SAURON Spectroscopy

To investigate the stellar populations of the NGC4546 UCD, and to allow a direct comparison to NGC4546 itself, we make use of SAURON IFU observations (Bacon et al. 2001). The SAURON datacube provides an on-sky coverage of $42.4'' \times 33.6''$ sampled with $0.94''$ lenslets, Figure 2 displays the log(flux) of the datacube (determined by summing the flux in each spatial element), with the UCD visible towards the top right. To produce the UCD spectrum, spatial elements within $1.5''$ of the centre of the UCD were coadded (12 in all). The sky, including NGC4546 diffuse light, was determined by averaging spatial elements within an annulus from 3 to $4''$ (36 in all). The final UCD spectrum covers the wavelength range 4825 to 5280 Å with a FWHM of $\sim$4.4 Å.

The recessional velocity of the NGC4546 UCD was determined using the same procedure as in Section 2.2. The measured velocity is consistent with that determined from our lower S/N SOAR spectroscopy. We also used the IDL code pPXF (Cappellari & Emsellem 2004) to provide an additional check of the UCD velocity and to confirm that the σ of the UCD is too low to measure (i.e., < 50 kms^{-1}).

To derive stellar population information from the UCD spectrum we measure Lick/IDS absorption line indices following the procedure outlined in Kuntschner et al. (2006). We degrade the SAURON spectrum with FWHM$\sim$4.4 Å to the resolution of the Lick/IDS system in the same wavelength range ($\sim$8.4 Å). We do not correct for the line of sight velocity distribution of the UCD, as its σ is less than 100 kms^{-1} and the correction is therefore negligible (Kuntschner 2004). Due to the limited wavelength coverage we can measure only three line indices, Hβ, Fe5015 and Mgb, using the standard definitions of Trager et al. (1998). The last step required to place our measured indices on the Lick/IDS system is to correct small systematic offsets due to continuum shape differences between the SAURON and Lick/IDS spectra. To do this we use the offsets of

Kuntschner et al. (2006, see Norris et al. 2006 for more details).

2.4 SOAR Imaging

We carried out BVR band imaging of NGC3923 and NGC4546 using the Goodman spectrograph in imaging mode. As a consistency check of our photometry, we also obtained SOAR/Goodman BVR imaging of the Sombrero UCD, which has previously published BVR imaging converted from the *HST* equivalent bands by Hau et al. (2009). Coadded images with 4×60s exposure time are shown in Figure 3. The imaging was binned 2×2 providing a pixel scale of $0.291''$, with seeing of $\sim$0.8 to $1.4''$.

In all cases the individual exposures were bias subtracted, flatfielded, and combined in IRAF using standard routines. As all of our UCD candidates are located within $3'$ of their host galaxies, care must be taken to remove the galaxy halo before accurate photometry can be achieved for the UCDs. To model the galaxy halos (and the sky background) the IRAF task MEDIAN was used to produce a median image, where each pixel was the median value of a 75×75 pixel box. The box size was chosen to be sufficiently large ($21.8'' \times 21.8''$) that the UCDs themselves did not affect the determination of the median. More details of this procedure and the method used to determine the optimum median box smoothing size are provided in Section 2.6.1.

After subtraction of the median image, the photometric measurements were carried out with SExtractor (Bertin & Arnouts 1996). The same procedure was used to reduce observations of the standard star field (SA104, Landolt 2009) observed prior to the galaxy imaging. Five standard stars were used to calculate the photometric zeropoints, providing zeropoint uncertainties of < 0.03 mag in all bands. Finally all photometry was corrected for Galactic extinction using the extinction maps of Schlegel et al. (1998).

To ensure that our photometry was accurately placed on standard photometric systems we compared our SExtractor output catalog of Sombrero galaxy GCs/UCD with the *HST* ACS photometry previously presented for these objects in Spitler et al. (2006) and Hau et al. (2009). In all three bands systematic offsets are <0.03 mag, validating the accuracy of our derived zeropoints.

2.5 IR Imaging

The UCDs of NGC4546 and the Sombrero are sufficiently luminous that they are detected in J, H, and K$_s$ by 2MASS (Skrutskie et al. 2006). For the UCDs associated with NGC3923, we have made use of archival K$_s$ imaging from the SOFI instrument on the 3.6 m ESO New Technology Telescope. These data have previously been described in Brown et al. (2003). Briefly, they comprise 30×30s exposures with a pixel scale of 0.292 arcsec pixel^{-1} and a field of view of 4.94×4.94 arcmin^2. All three NGC3923 UCD candidates are located within this field of view. We reduced the data in IRAF using standard routines to subtract the dark, produce and apply a flat field constructed from the object frames, combine the individual exposures with a sigma clip, and carry out a median image subtraction (box size 50×50
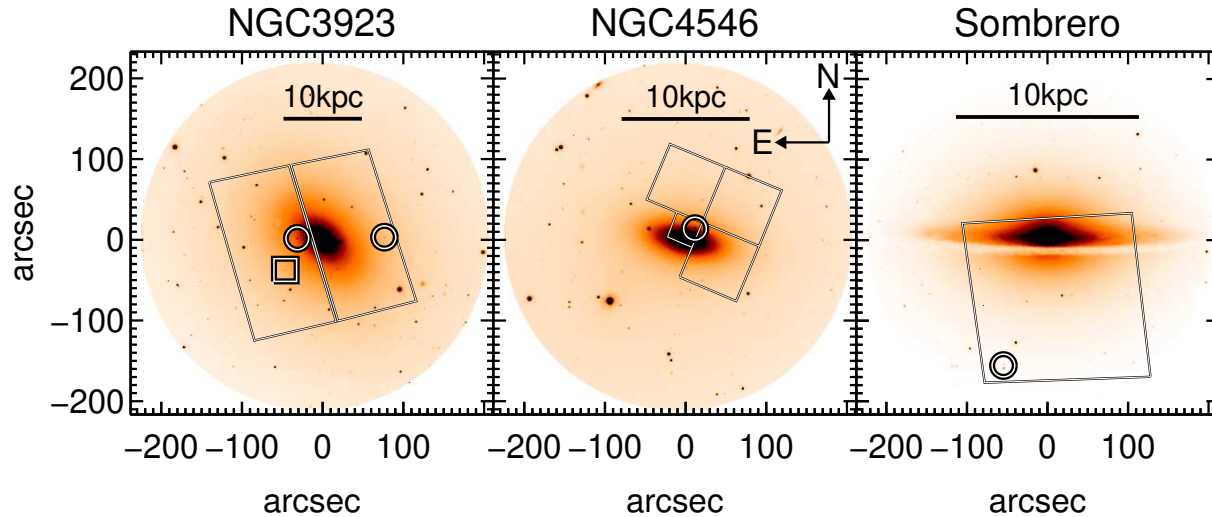
Figure 3. SOAR/Goodman V-band images showing the location of our confirmed field/group UCDs (circles) as well as the candidate third NGC3923 UCD (square), relative to their host galaxies. The *HST* ACS or WFPC2 footprints are also indicated. The solid black line in each panel denotes 10 kpc at the assumed distance of the galaxies.

pixels) to remove the galaxy halo and sky. The zero point of the image was determined by comparison with 2MASS photometry of 9 isolated stars within the FOV. Finally, a small correction for Galactic extinction was applied based on the dust extinction maps of Schlegel et al. (1998).

2.6 HST Imaging

Table 2 lists the *HST* imaging available for our three target galaxies. For NGC4546 and the Sombrero galaxy we make use of *HST* imaging only to derive structural properties of the UCDs. This is because only one band of *HST* imaging is available for NGC4546 and because the photometric properties of the Sombrero UCD have been extensively discussed previously in Hau et al. (2009).

The GC system of NGC3923 has previously been examined with *HST* ACS Wide Field Camera photometry comprising 1140s in F606W ($\sim$V) and 978s in F814W ($\sim$I). The ACS WFC has a pixel scale of $0.05''$, which at the distance of NGC3923 equates to 5.15 pc/pixel. These data have been described in detail in Sikkema et al. (2006) and Cho (2008). However, in both cases the UCD candidates appear to have been ignored, presumably because they are clearly resolved and their luminosities are too high to be standard GCs. We therefore re-examined these data to provide accurate V and I band photometry as well as structural information for our candidate UCDs and the GCs of NGC3923.

2.6.1 Background Subtraction

The determination of integrated magnitudes and especially structural parameters for GCs and UCDs depends sensitively on the careful removal of the host galaxy halo light. We have therefore applied the same median background removal approach mentioned in Section 2.4 to the *HST* data as well. The choice of median box size for the smoothing is particularly critical. Too small a box size results in the subtraction of UCD flux, while too large a box size results

in an inaccurate removal of the host galaxy halo. We therefore investigated the optimum choice of median box size for our imaging. To do this for NGC3923, for example, we produced median images of the F606W imaging of NGC3923 with a range of box sizes of between 5×5 and 301×301 pixels (25.75×25.75 to 1550×1550 pc). We then subtracted these smoothed models from the original image and measured the total magnitude of each of our three NGC3923 UCD candidates contained within a 250 pc radius (curve-of growth analysis shows that no UCD luminosity is expected beyond this radius, see next section). Figure 4 displays the result of this analysis. The total magnitude of each UCD converges to a constant value for box smoothing sizes of 251 pixels or more. To determine the size of sky residuals left by each smoothing box we also measure the residual sky counts in a region adjacent to each of the three UCD candidates. For all three NGC3923 UCD candidates a 251×251 pixel smoothing box offers the optimum choice of box size, providing the correct total UCD flux and lowest sky residuals. The corresponding values for the NGC4546 and Sombrero UCDs are similar at 201×201 and 301 × 301 pixels respectively. We caution that this fortunate result will not hold true in all cases: the optimum choice of smoothing box depends on several factors, including UCD size and structure as well as the behaviour of the galaxy background and the proximity of the object to the edges of the chip. In general for UCDs located near to galaxies it is necessary to determine the optimum smoothing scale for each UCD candidate individually. Figure 5 displays an example of the result of this approach for the region around NGC3923-UCD1; as can be seen the galaxy halo is very effectively removed.

2.6.2 Integrated Magnitudes

We used the curve of growth method to determine total magnitudes, applying extinction corrections following Schlegel et al. (1998) and converting between HST and Johnson-Cousins filter systems using the method of Sirianni et al. (2005) with a G2V spectral energy distri-
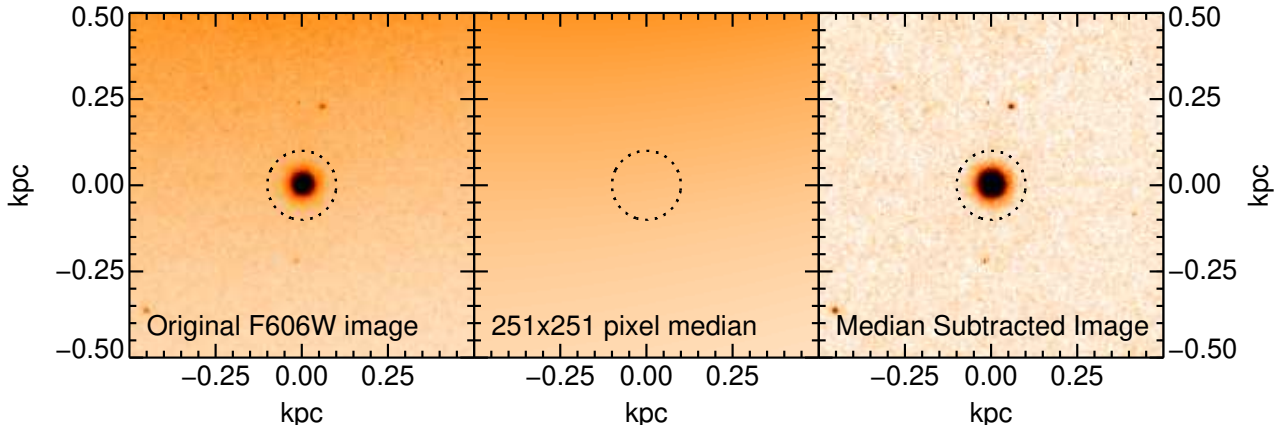
Figure 5. Demonstration of the median subtraction of the NGC3923 halo. The left panel is the input ACS F606W image, centred on NGC3923 UCD1. The central panel is the 251×251 pixel median image. The right panel is the median subtracted image used to measure UCD photometry. The dashed circles in all three panels show the maximum extent of UCD1 determined by a curve of growth analysis.
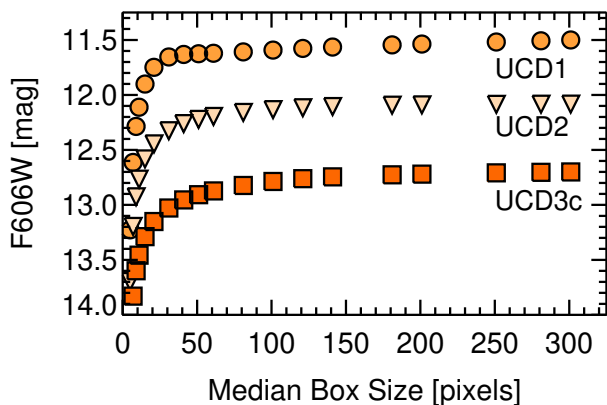

Figure 4. Demonstration of how the choice of median smoothing box size affects the total magnitude summed within 250 pc (48.5 pixels) of our NGC3923 UCDs. A box size of 251×251 pixels is sufficiently large to be unaffected by the presence of the UCDs.

bution. The *HST* derived magnitudes are given in Table 3 and agree with SOAR photometry where available. As only single-band *HST* photometry is available for NGC4546 we do not convert its *HST* photometry to the standard Johnson-Cousins system. Our ground based photometry is therefore used in all analyses of the NGC4546 UCD that rely on integrated magnitudes. For analyses of integrated magnitudes involving the Sombrero UCD we make use of the photometry obtained by Hau et al. (2009). We make no correction for internal extinction by the host galaxies, as none of our UCD candidates are located near obvious dust features.

2.6.3 NGC3923 GC Photometry

We have reexamined the GC system of NGC3923 in order to provide a sample of GCs to compare to our NGC3923 UCDs. The data used are the same *HST* ACS data described above, which have been used previously to study the GC system of NGC3923 by Sikkema et al. (2006) and Cho (2008).

Our reanalysis of the data followed the procedure of Cho (2008); we ran SExtractor on the MultiDrizzle reduced frames with the selection parameters set to a minimum area of 5 pixels and a significance of at least 3σ above the background computed in a 32×32 pixel box. The flux within a 3 pixel radius around each of the detected objects was then measured and an aperture correction made to correct the photometry to an infinite aperture (0.321 mag in F606W and 0.367 mag in F814W). As in the UCD case the photometry was corrected for Galactic extinction and the measured instrumental magnitudes were converted to V and I.

The major difference between our reanalysis and the earlier works is in the way potential GCs/UCDs are selected. Unlike Sikkema et al. (2006) and Cho (2008) we do not require that all objects must be close to unresolved to be classed as GCs, nor do we apply a simple upper magnitude limit for inclusion in the sample. This is in marked contrast to studies of extragalactic GCs in general, where an upper magnitude limit close to that of ωCen is often applied to reduce contamination by Milky Way stars. It is our belief that this approach has most likely led to the misclassification of many potential UCDs as background galaxies or foreground stars in photometric surveys of extragalactic GCs.

Accepting partially resolved GC candidates is supported by the fact that five spectroscopically confirmed GCs (Norris et al. 2008, 2011 in prep.) are significantly extended, with SExtractor class_star values of 0.2 to 0.75, well below the limit imposed by Cho (2008) of 0.9. However, we do limit the GC analysis to objects fainter than $M_V > -11.0$. Objects brighter than this must be resolved to be included in the UCD analysis. $M_V = -11.0$ is where the UCD luminosity-size trend ensures that bona-fide UCDs are large enough to be resolved at the distance of NGC3923 (see Section 3.3).

To reduce contamination by stars and background galaxies we restricted our GC/UCD sample to objects with ellipticities less than 0.25, and imposed a colour cut of 0.7 < V–I < 1.5. This selection recovered all spectroscopically confirmed GCs, as well as the three NGC3923 UCDs. We restrict further analysis to objects with I < 23.8 (0.5 mag brighter than the 90% completeness limit, see Appendix B), which ensures that we are dealing with the regime where incompleteness is negligible in both V and I. In total we find

Name	R.A. [h:m:s]	Dec. [d:m:s]	B [mag]	V [mag]	R [mag]	I [mag]	K_s [mag]	V_{helio} [kms^{-1}]
NGC3923 UCD1	11:51:04.1	−28:48:19.8	20.08±0.10	19.21±0.04*	18.73±0.04	18.10±0.04*	16.26±0.06	2096.9±17.8
NGC3923 UCD2	11:50:55.9	−28:48:18.4	20.49±0.12	19.71±0.05*	19.32±0.05	18.70±0.05*	17.10±0.10	1500.5±44.2
NGC3923 UCD3c	11:51:05.2	−28:48:58.9	21.18±0.16	20.35±0.07*	19.95±0.07	19.38±0.07*	18.07±0.17	-
NGC4546 UCD1	12:35:28.7	−03:47:21.1	18.57±0.05	17.64±0.04	17.15±0.03	-	14.86±0.17	1255.9±24.0
Sombrero UCD1	12:40:03.1	−11:40:04.3	18.37*	17.46*	16.88*	-	14.70±0.11	1293.1±9.5

Table 3. Basic properties of four confirmed UCDs and one more UCD candidate in the three systems studied. B,V,R and I magnitudes are from SOAR/Goodman or *HST* imaging (*HST* magnitudes denoted by *). The optical photometry and recessional velocity for the Sombrero UCD is from Hau et al. (2009). All magnitudes have been corrected for foreground dust extinction following Schlegel et al. (1998). K_s data for NGC4546 and the Sombrero are from 2MASS; K_s data for NGC3923 are from our reduction of archival NTT imaging. Recessional velocities are from SOAR/Goodman except for the Sombrero UCD.

549 objects that meet our criteria and that we provisionally classify as GCs in addition to the three UCDs.

2.6.4 UCD Structural Modelling and Half Light Radii

We used GALFIT (Peng et al. 2002) to fit King and Sérsic models to $5''\times5''$ (515×515 pc) images of the NGC3923 UCDs. Background and foreground objects and bad pixels were masked, and position dependent artificial PSFs were constructed using TINYTIM (Krist 1995). Each PSF was $4''\times4''$ in size and was produced using a G2V template. We remove sky and galaxy background as described in Section 2.6.1. We also experimented with different median smoothing box sizes, finding that the resulting GALFIT model is not significantly affected as long as the box size is several times the half-light radii of the objects under study.

We fit both standard (King 1962) and generalised King profiles (Elson 1999), which typically fit GCs well. We also fit Sérsic (Sersic 1968) and generalised King + Sérsic models. In practice the Sérsic component mostly helps to fit unresolved core features. Note that in all cases the cores are unresolved (or the objects lack cores), so derived parameters such as central surface brightness are unreliable. However, properties that depend on large-scale modelling such as half-light radii are relatively robust. These radii underlie our analysis in Section 3.3.

To determine the intrinsic half-light radii R_e of our UCDs in the absence of PSF effects we used GALFIT to reconstruct the best fit King + Sérsic models without the PSF convolution. The half-light radii were then determined by direct integration of the model profiles. We quote the average of the radii determined from the F606W and F814W images for the NGC3923 UCDs. For the NGC4546 UCD only the F606W image is available. For the Sombrero UCD we quote the half-light radius determined by Hau et al. (2009), but find that our half-light radius for this UCD is consistent with theirs within the quoted errors (12.9 ± 2.0 pc compared to 14.7 ± 1.4 pc).

We are unable to place any strong constraints on the presence of low surface brightness envelopes around our UCDs. In the case of NGC4546 this is because the photometry is too shallow. For the NGC3923 UCDs it is due to the strong shells of NGC3923 which complicate accurate galaxy background removal.

2.7 Stellar Mass Estimates

To produce stellar mass estimates for the UCDs we use a modified version of the stellar mass estimation code first presented in Kannappan & Gawiser (2007) and later updated in Kannappan et al. (2009). Briefly, the code fits photometry from the Johnson-Cousins, Sloan, and 2MASS systems with an extensive grid of models from Bruzual & Charlot (2003) (the updated 2009 models which include the effects of asymptotic giant branch stars) assuming a Salpeter initial mass function (IMF). The derived masses are then rescaled by a factor of 0.7 to approximate the "diet" Salpeter IMF of Bell & de Jong (2001). Each collection of input UCD photometry is fit by a grid of model SSPs with ages from 25 Myr to 13.5 Gyr and metallicity Z = 0.0001 to 0.05. Unlike Kannappan et al. (2009) our input models are pure SSPs, with no composite models, and no extinction. The derived stellar mass is determined by the median and 68% confidence interval of the mass likelihood distribution binned over the grid of models. We also measure stellar masses for the host galaxies using catalog Hyperleda + 2MASS photometry and exactly the same grid of models as in Kannappan et al. (2009) to facilitate comparison of galaxy mass scales (Section 4.1).

The estimation of stellar masses is inherently uncertain. In fact, the use of different estimation methods or SSP models can lead to changes in the derived masses of up to factors of two, even when assuming the same IMF (Kannappan & Gawiser 2007). This problem is compounded by the fact that the correct choice of IMF for UCDs is still a matter of debate (see e.g. Mieske et al. 2008a; Chilingarian et al. 2010). We therefore caution that UCD stellar mass estimates are subject to systematic uncertainties in overall normalization at a factor of ∼3 level, which should not strongly affect comparisons within a given sample analyzed uniformly.

3 RESULTS

In this section we present several basic observational results, which are discussed in a common framework in Section 4. We examine the orbital characteristics, stellar populations, and statistical distributions of our UCDs to demonstrate that (i) the candidate UCDs are bona-fide and associated with their apparent hosts, (ii) their ages, statistics in relation to the GC luminosity function, and apparent decay timescales are
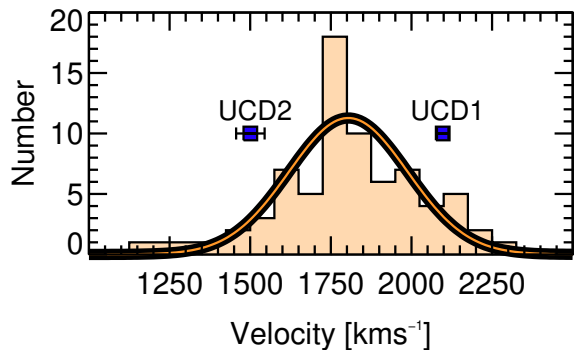
Figure 6. Histogram of NGC3923 GC velocities measured by Norris et al. (2008, 2011 in prep). Overplotted are the best-fit Gaussian to the GC population and the velocities of the two confirmed NGC3923 UCDs (squares).

distinct, pointing to different formation mechanisms for the NGC3923 and NGC4546 UCDs, and (iii) our data provide no evidence yet for dependence of UCD frequency on galaxy environment. We argue that UCDs that form as giant globular clusters (GGCs), as in NGC3923, emerge with distinct structural properties above a mass of 2×10^6 M$_\odot$ and likely cannot exceed a mass of 7×10^7 M$_\odot$, while UCDs that form as stripped nuclei, as in NGC4546, can exist at all masses.

3.1 UCD Recessional Velocities & Survival Times

As detailed below, recessional velocities derived from SOAR spectroscopy confirm physical association between the UCDs and their host galaxies. Examination of the velocities and projected radii of the UCDs indicates a possible difference in dynamical friction decay timescale between the NGC4546 UCD and the other UCDs.

In the case of NGC3923 the GC velocity distribution has been measured by Norris et al. (2008) and will be studied in detail in a forthcoming paper (Norris et al. 2011, in prep.). As Figure 6 shows, the velocities of NGC3923-UCD1 and UCD2 (2096.9±17.8, 1500.5±44.2 kms^{-1}) are in excellent agreement with those of the GC system of NGC3923 (as well as NGC3923 itself, which has V=1739 kms^{-1}) confirming physical association. In further analyses we assume that UCD3c is also physically associated with NGC3923. The recessional velocity of NGC4546 is 1050 ± 9 kms^{-1}, therefore our measured recessional velocity for NGC4546-UCD1 of 1255.9±24.0 kms^{-1} implies a high likelihood that these two objects are physically associated. Finally, the UCD of the Sombrero has a relative velocity (269±11 kms^{-1}) that is slightly larger than the one standard deviation of the GC velocity distribution of the Sombrero, making it likely that this UCD is bound to the Sombrero galaxy (Hau et al. 2009).

Making the simplifying assumption of circular orbits, and assuming that the projected separations of the UCDs from their host galaxies are of the same order of magnitude as the true physical separations r_i, we expect their survival times to obey the dynamical friction timescale from equations 8.2 and 8.12 of Binney & Tremaine (2008), applicable for small satellites of massive galaxies:

$$t_{\mathrm{fric}} \quad = \quad \frac{19 \text{ Gyr}}{\ln\Lambda} \left(\frac{r_i}{5 \text{ kpc}} \right)^2 \frac{\sigma}{200 \text{ kms}^{-1}} \frac{10^8 \text{ M}_\odot}{M}. \qquad (1)$$

Here σ is the velocity dispersion of the host galaxy, M is the total mass of the UCD (as determined in Section 3.3.3), and

$$\ln\Lambda \quad = \quad \ln\left(\frac{b_{\max}}{r_h} \right). \qquad (2)$$

We assume that r_h, the half-mass radius of the UCD, is equal to r_e, the half-light radius of the UCD, and that $b_{\max}$ can be approximated by the observed projected separation between the UCD and host galaxy centre.

The resulting dynamical friction decay timescales for our UCDs are provided in Table 4. It is intriguing that the UCDs of NGC3923 and the Sombrero have long dynamical friction decay timescales of at least 7 Gyr, and usually several Hubble times, whereas the UCD of NGC4546 is only expected to survive for around 0.5 Gyr. Objects that are already long-lived at the present would not be expected to have short dynamical friction decay timescales on average, as only a handful should be caught fortuitously at the end of their lives. This implication is borne out by the fact that none of the the GC candidates (modulo the ones lost due to the bright background in the very centre) detected by the HST have computed decay timescales of less than 8 Gyr. Moreover, based on galaxy and UCD/GC masses alone, the NGC3923 UCDs have normal dynamical friction decay timescales, i.e the UCDs of NGC3923 appear to be drawn from the same population as the GCs of NGC3923. In contrast, after correcting for differences in host galaxy mass, the NGC4546 UCD is consistent with outliers comprising only 1.8% of the distribution of cluster mass vs. decay time. Nonetheless, with only a handful of UCDs we cannot be sure that the projected quantities reflect the true values.

3.2 UCD Stellar Populations

In this section we examine the stellar populations of our UCDs. In the case of the NGC4546 UCD we utilise SAURON spectroscopy to measure its age, metallicity, and alpha-element enhancement, which differ significantly from those of the host galaxy. For the Sombrero, the stellar population information provided by Hau et al. (2009) and Larsen & Brodie (2002) indicates similar UCD and GC properties, with both having old ages (age > 10 Gyr) consistent with those measured for the centre of the Sombrero by Sánchez-Blázquez et al. (2006). Unfortunately we currently lack spectroscopy of sufficient S/N to examine the stellar populations of the NGC3923 UCDs. However, the NGC3923 GCs, including several which are marginally resolved by *HST* and hence may prove to be UCDs, have been studied by Norris et al. (2008), with all studied GCs consistent with being old. Furthermore, a general examination of the position of UCDs, GCs, and dwarf nuclei in colour-magnitude space reveals that all three populations significantly overlap. In particular, blue UCDs and dwarf nuclei extend the observed "blue tilt" or mass-metallicity relation of blue GCs.

3.2.1 The Young UCD of NGC4546

We find that the single UCD of NGC4546 is considerably younger than its host galaxy (3.4 vs. 10.7 Gyr), with significantly reduced alpha-element enhancement ($\sim$0 vs. 0.3), implying extended star formation.

Figure 7 displays the Lick/IDS absorption line indices determined for the UCD in Section 2.3, as well as values measured for the diffuse light of NGC4546 at $R_e/8$ and R_e by Kuntschner et al. (2006, 2010). Overplotted are the SSP models of Thomas et al. (2003, 2004). For index combinations sensitive to the effects of $[\alpha/Fe]$ (those with Mgb) we overplot two choices of $[\alpha/Fe]$, the black grid has $[\alpha/Fe]$=0.0, appropriate for the UCD, the red grid has $[\alpha/Fe]$=0.3, appropriate for the NGC4546 diffuse light. As Figure 7 demonstrates the implied stellar population parameters of age, [Z/H] and $[\alpha/Fe]$ are consistent for all choices of index combination. By eye the UCD appears to be relatively young ($\sim$3 Gyr), metal rich ([Z/H] $\sim$ solar) and with $[\alpha/Fe]$ close to solar. In contrast, the diffuse light of NGC4546 is old, displays a negative metallicity gradient, and is alpha-enhanced.

In order to determine a more definitive best-fit SSP we use the χ^2-minimisation approach of Proctor et al. (2004). To carry out the fit we first interpolate the SSP models of Thomas et al. (2003, 2004) to a finer model grid, then we perform a χ^2-minimisation on the resulting age, [Z/H] and $[\alpha/Fe]$ space. Errors come from 50 Monte-Carlo resimulations of the input data within the measured index errors. The final best-fit SSP model for the NGC4546 UCD is: age $= 3.4^{+1.7}_{-1.2}$ Gyr, [Z/H] $= 0.21 \pm 0.14$, and $[\alpha/Fe] = -0.01 \pm 0.08$. The equivalent SSP parameters for the diffuse light of NGC4546 as measured by Kuntschner et al. (2010) at R_e are: age $= 11.7^{+1.1}_{-1.0}$ Gyr, [Z/H] $= 0.13 \pm 0.02$, and $[\alpha/Fe] = 0.31 \pm 0.05$. At $R_e/8$ the parameters are: age $= 10.7^{+1.0}_{-0.9}$ Gyr, [Z/H] $= -0.13 \pm 0.02$, and $[\alpha/Fe] = 0.27 \pm 0.04$. We discuss the implications of these results in Section 4.

3.2.2 Indistinguishable Colour Magnitude Diagrams and Blue Tilts for GCs, UCDs, and Galaxy Nuclei

The "blue tilt" is the observation that in massive galaxies the more luminous blue population GCs are systematically redder (more metal rich) than their lower luminosity counterparts (e.g. Strader et al. 2006; Mieske et al. 2006a; Harris et al. 2006; Peng et al. 2009; Forbes et al. 2010). In this section we demonstrate that blue GCs, blue UCDs, and dwarf nuclei display the same blue tilt in their colour-magnitude relations. Furthermore, we observe that the nuclei of dwarf galaxies display identical colour-magnitude behaviour to that of GCs at lower mass, and UCDs at higher mass (including following the same steepening of the tilt above $\sim M_V$=-10). Assuming that the observation that GCs, UCDs and dwarf nuclei display indistinguishable blue tilts is not a conspiracy of the age-metallicity degeneracy and that all three types of object have similar ages, this striking correspondence can be interpreted in three subtly different ways. 1) Dwarf nuclei are merely GCs/UCDs that have sunk to the centre of their host galaxies. 2) Blue GCs/UCDs are the stripped nuclei of dwarfs. 3) The same physics of self enrichment acting on all three object types leads independently to the same mass-metallicity relation. The implications of these explanations will be discussed in detail in Section 4.
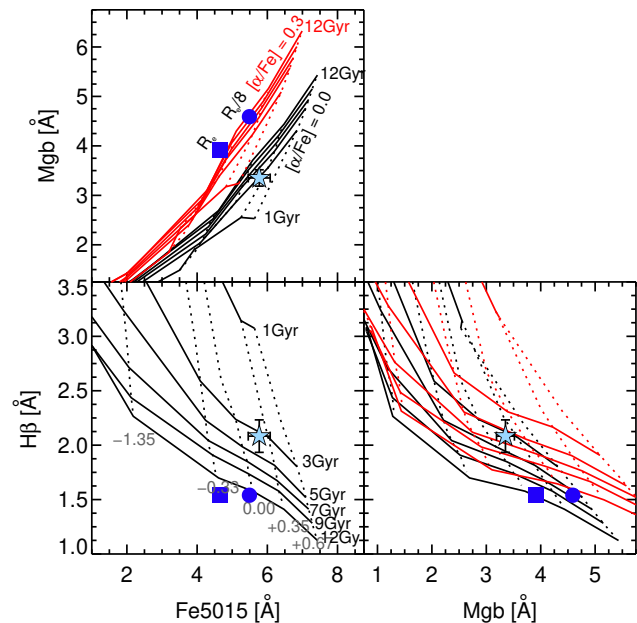

Figure 7. Index-index plots for the NGC4546 UCD (blue star), measured as described in the text, plus the diffuse light of NGC4546 measured at $R_e/8$ (blue circle) and R_e (blue square) by Kuntschner et al. (2006). Overplotted are the model grids from Thomas et al. (2003, 2004) spanning the age range of 1 to 12 Gyr and [Z/H] from -2.25 to $+0.67$. For index-index combinations with sensitivity to $[\alpha/Fe]$ variation we overplot two choices of $[\alpha/Fe]$, appropriate for the UCD ($[\alpha/Fe] = 0.0$, black grid) and the NGC4546 diffuse light ($[\alpha/Fe]$=0.3, red grid).

Figure 8 displays the NGC3923 GC/UCD colour-magnitude diagram. Bimodality in the colours of the GC system is detected with high significance ($>$99%, as estimated using the KMM method of Ashman et al. 1994a). The measured peaks of the blue and red GC populations of V–I $= 0.97$ and 1.23 are close to those found for the GC systems of ellipticals such as M87 (V–I $= 1.0$ & 1.2, Tamura et al. 2006). They are also consistent with those determined previously for the NGC3923 GC system by Cho (2008).

Intrigued by the possible existence of a "blue tilt" in the blue GCs of NGC3923 we estimated the significance of such a trend. A description of the procedure used is provided in Appendix A. The tilts measured in this investigation can be seen in Figure 8 as the dashed lines. A blue tilt in the blue GC population is detected at $> 3\sigma$ confidence, with a slope indistinguishable from that displayed by the GCs around M87 (Peng et al. 2009). No evidence is found for a corresponding tilt in the red GC system.

Of particular interest in Figure 8 is the fact that the NGC3923 UCDs are all consistent with an extrapolation of the measured blue tilt (all three are within 1.5σ of the best fit trend). This perhaps indicates a continuation of this phenomenon into the UCD mass range. In order to investigate this behaviour further we have constructed a catalog of published UCD photometry and compared this to the behaviour of the M87 GCs observed by Peng et al. (2009); see Figure 9. We choose M87 as our comparison sample because of the very high quality V and I band photometric measurements of 2250 GCs provided by Peng et al. (2009). We note that the measured value of the blue tilt varies from galaxy
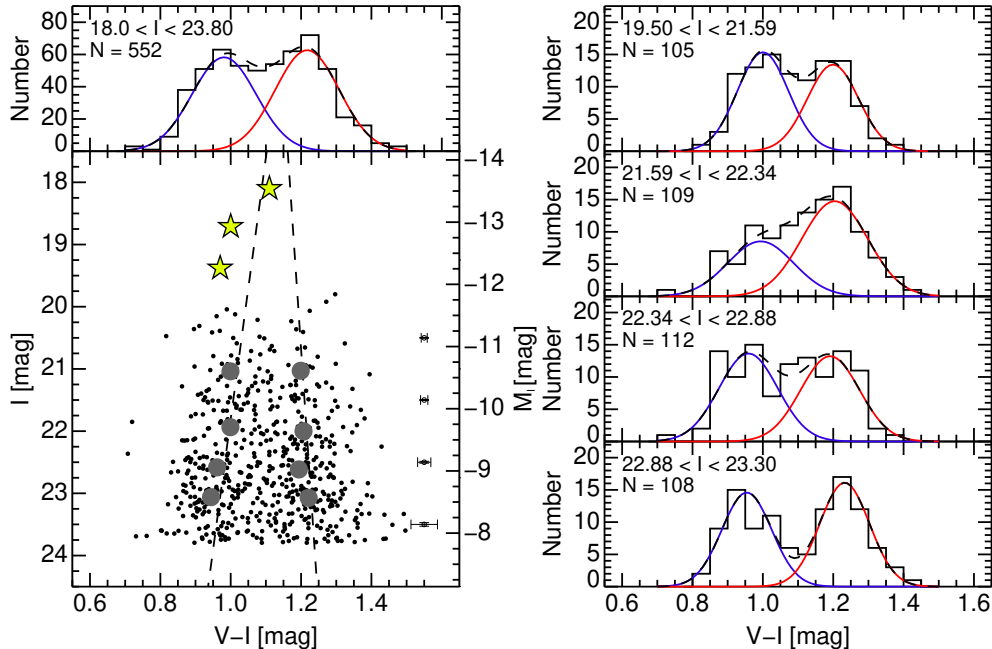
Figure 8. Left Panel : Lower: V–I colour-magnitude diagram of 549 NGC3923 GCs (small black dots) and UCDs/UCD candidates (yellow stars). Large filled circles denote the positions of the peaks of the best-fit KMM (Ashman et al. 1994b) two Gaussian models to the GC colour distributions in four magnitude bins. The dashed lines denote the best-fit linear relations to the large filled circles. Upper: The upper panel shows the total colour distribution of all 552 objects (black histogram), and best-fit blue and red GC colour distributions and their sum (blue, red and black lines). **Right Panel** : Same as in upper left panel but for the four magnitude bins into which the GCs have been divided for the examination of the blue tilt (see Section 3.2.2 and Appendix A).

to galaxy with a dependence on galaxy mass (Mieske et al. 2010). However, almost all of the UCDs to be discussed here (except the NGC4546 UCD) are likely associated with high-mass galaxies (those defined by Mieske et al. 2010 as having $M_* > 5 \times 10^{10}$ $M_\odot$), which Mieske et al. (2010) find to have the largest magnitude blue tilts. Therefore, the scatter added due to the possible superposition of several varying UCD blue tilts should be relatively small.

The UCD photometry compiled for Figure 9 consists of our field/group UCDs plus Virgo (Haşegan et al. 2005; Firth et al. 2008; Evstigneeva et al. 2008), Fornax (Mieske et al. 2004; Firth et al. 2007, 2008; Evstigneeva et al. 2008), Centaurus (Mieske et al. 2009) and Hydra (Misgeld et al. 2008) cluster UCDs/DGTOS/CSSs[2] observed directly in V and I or in equivalent bands (g/r/i or g/z) converted into V and I (using the SDSS to Johnson-Cousins conversions of Lupton[3], or the conversions of Evstigneeva et al. 2008, assuming the UCDs are 11–13 Gyr old). To check the accuracy of the conversions to V/I, we compare native V/I magnitudes to those derived from the conversions for a sample of ∼20 UCDs that have both V/I and g/r/i or g/z observations. We find small δV, δI < 0.1 mag systematic offsets, which we subtract off all converted V/I magnitudes to ensure consistent photometry. The dispersion in the native V/I vs. converted V/I photometry is around 0.1 mag, making this source of error comparable to that of the standard photometric errors. To place the NGC4546 and Sombrero UCDs (that

lack I band photometry) on the same figure we adopt a different approach. We predict V and I fluxes from the measured SSP ages and metallicities found in Section 3.2.1 for NGC4546 and by Hau et al. (2009) for the Sombrero UCD, making use of the SSP models of Maraston (2005). This method reproduces colours within 0.1 mag for all of the optical colour combinations we have access to (B–V, V–R and B–R).

On Figure 9 we also overplot a sample of dwarf nuclei. The dwarf nucleus measurements are provided by Côté et al. (2006) for Virgo dwarfs (converted from g–z using the approach described above) and Lotz et al. (2004) for a sample of Virgo, Fornax and Leo group dwarfs (observed in V/I).

Focusing on the left panel first, of immediate note is the fact that there is considerable overlap in magnitude between objects classified as GCs and those classified as UCDs. This is likely due to the fact that the *HST* imaging necessary to securely distinguish UCDs and GCs on the basis of size does not exist for all objects; many of these lower luminosity UCDs are in all probability bright intra-cluster GCs.

Also of interest is the observation that the UCDs seem to continue the colour-magnitude trends of GCs. The vast majority of UCDs lie within the lower and upper colour limits of the GCs. The bluer UCDs, as seen for NGC3923 in Figure 8, also display a blue tilt similar to that of the blue GCs, including a steepening of the relation for M_V brighter than –10. This behaviour is strikingly reminiscent of that seen for the most luminous blue GCs of eight brightest cluster galaxies studied by Harris et al. (2006). It is also in reasonable agreement with the self-enrichment model of GC formation of Bailin & Harris (2009) (see their Figure 7). In

---

[2] In the future we will refer to all UCDs/DGTOs/CSSs as UCDs.
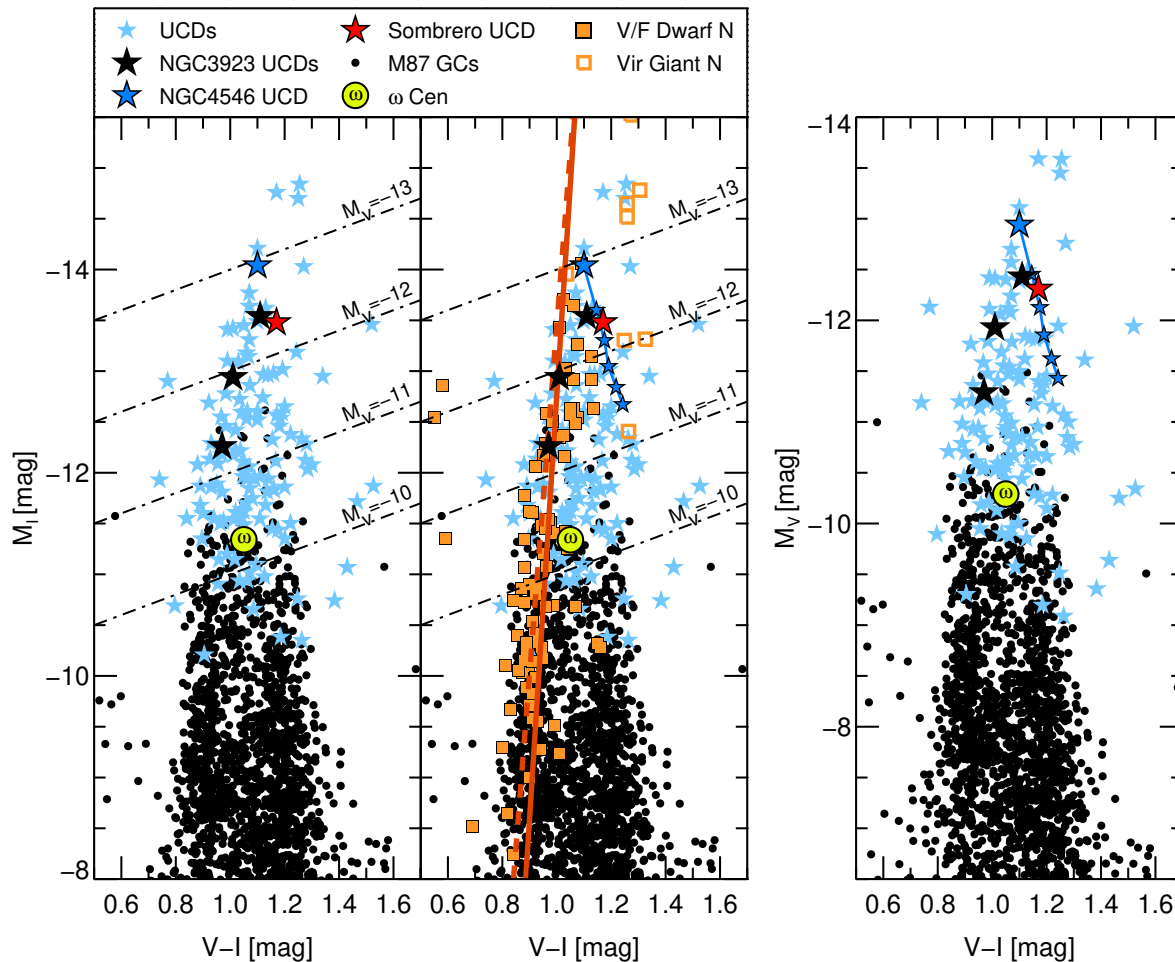[3] www.sdss.org/dr7/algorithms/sdssUBVRITransform.html

Figure 9. Colour-Magnitude Diagrams for M87 GCs (black dots), UCDs (stars), and Virgo and Fornax cluster galaxy nuclei (squares). The solid black stars denote our NGC3923 UCDs. The large blue star is the predicted position of the NGC4546 UCD based on its spectroscopically measured stellar population (see Section 3.2.1), while the small blue stars are predictions for the evolution of the NGC4546 UCD for ages of 5, 7, 9, 11 and 13 Gyr. The red star is the predicted position of the Sombrero UCD based on the measured SSP from Hau et al. (2009). Orange squares represent Virgo, Fornax and Leo group dwarf nuclei from Côté et al. (2006) and Lotz et al. (2004), with filled/open squares representing nuclei of galaxies with M_B fainter/brighter than –17.6 respectively. The M87 GC photometry is from Peng et al. (2009), and the UCD photometry is from the catalog of UCDs described in the text. The solid line is the best-fit "blue tilt" relation found for M87 blue GCs by Peng et al. (2009). The dashed line is the best-fit relation found for the nuclei of galaxies with M_B fainter than –17.6 (identical within the errors).

the Bailin & Harris model the change in slope is a manifestation of the fact that clusters with mass $> 10^6$ $M_\odot$ ($M_V \sim$ –9) retain a significant amount of supernovae ejecta, leading to substantial self-enrichment.

Turning to the middle panel of Figure 9, we note that dwarf nuclei trace the behaviour of the blue GCs and UCDs over six magnitudes in I, even displaying a similar break in slope (at $M_I \sim$–11) . When we fit a linear relation to the dwarf nuclei over the same magnitude range as used by Peng et al. (2009) to determine M87's blue tilt (–12 < M_I < –7.8), the resulting fit is statistically indistinguishable from that of the M87 blue GCs. Also intriguing is the difference in behaviour between the nuclei of dwarf and giant galaxies. The dwarf galaxy nuclei display a strong blue tilt, while the giant galaxy nuclei are redder with fairly constant colour. Although the M_B = –17.6 mag dwarf/giant separator used by Côté et al. (2006) was originally a morphologically defined separation between dwarf and giant Virgo galaxies, it

also corresponds to the "gas-richness threshold mass" scale that lies at the transition point of several galaxian properties (Kannappan et al. 2009). Using Nearby Field Galaxy Survey Tully-Fisher relation data (Kannappan et al. 2002) we find that M_B = –17.6 corresponds to a circular rotation velocity of $V_{circ} \cong 120$ kms^{-1} for the red/old galaxies expected in clusters. This mass scale is where Garnett (2002) and Dalcanton et al. (2004) observe sharp changes in [Fe/H] and dust lane structure, apparently simultaneously with strong shifts in gas richness (Kannappan & Wei 2008, updating Kannappan 2004) and in galaxy structure (Kannappan et al. 2009, and references therein). The colour dichotomy of galaxy nuclei therefore appears to be another important transition in galaxian properties occurring at the threshold mass scale. Notably, the expected colour-magnitude evolution of the young NGC4546 UCD may move it into the regime of red nuclei in ~4 Gyr (see Section 4.1).
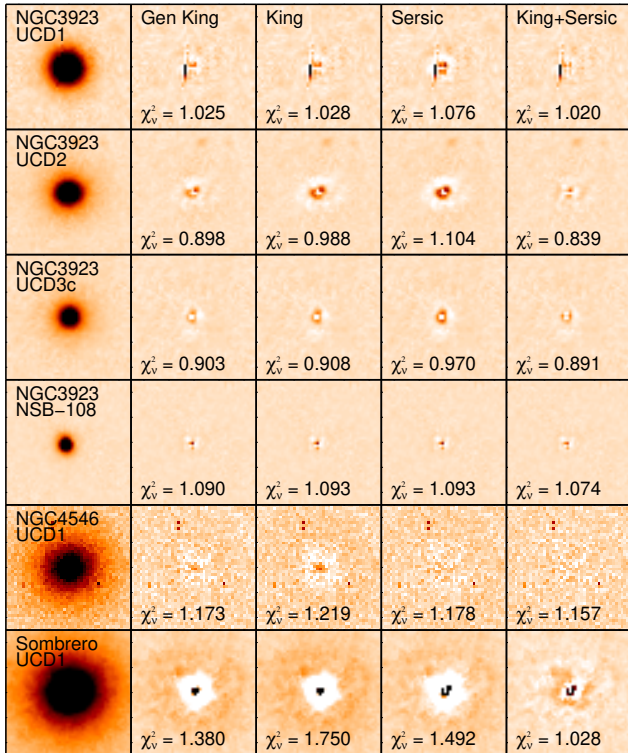
Figure 10. Field/Group UCDs and NSB-108, one of the brightest spectroscopically confirmed NGC3923 GCs. The first column displays the original F606W images (F625W for the Sombrero UCD). The remaining columns show the residuals after subtracting the PSF-convolved GALFIT models. All images are $2.5'' \times 2.5''$.

3.3 UCD Structural Properties

In this section we examine the structures of our UCDs. We find that they are reasonably fit by GC-like King profiles. We also find that the half-light radii of our UCDs, $12 - 25$ pc, are considerably larger than those of typical GCs. As seen in previous work, we find that UCDs display luminosity-size and mass-size trends, in the sense that more luminous/massive UCDs are more extended. In contrast, GCs have roughly constant size over $\gtrsim 2$ dex in luminosity/mass. Additionally, we find a striking and previously unreported correspondence between the luminosity at which the M_V-size trend of UCDs commences and the luminosity at which the "blue tilt" (i.e. M_V-metallicity trend), becomes most pronounced, which we jointly label the "scaling onset luminosity".

3.3.1 UCD Profile Shapes

Figure 10 shows result of fitting structural models to the UCDs and a bright ($M_V = -9.9$) NGC3923 GC spectroscopically confirmed by Norris et al. (2008). As expected, the fit to the bright GC is unconstrained due to its marginal resolution. It is very difficult to draw firm conclusions regarding the structures of the UCDs: they are all better fit by generalised King profiles or King+Sérsic profiles than by standard King or Sérsic models, but not significantly. There is no evidence for any particular UCD displaying a different structure from any other. In general, while the GALFIT modelling is useful in determining half-light radii for the

UCDs (see Section 2.6.4), the structures of our UCDs do not provide any clues to possible different formation scenarios within the UCD population.

3.3.2 UCD Half-Light Radii

Table 4 presents the half-light radii of our UCDs. The NGC3923 UCDs have almost constant half-light radii of around 13 pc, the Sombrero UCD also has a similar half-light radius of 14.7 pc (Hau et al. 2009), and the NGC4546 UCD is more extended at around 25 pc. All five UCDs are therefore significantly larger (as well as more luminous) than Milky Way GCs, which have half-light radii of around 3.2 pc (Rejkuba et al. 2007). These half-light radii place these objects squarely within the range displayed by Virgo and Fornax UCDs as measured by Evstigneeva et al. (2008).

3.3.3 UCD Luminosity/Mass-Radius Relations

The left and centre panels of Figure 11 demonstrate that our field/group UCDs fall along the same luminosity-size relation defined by cluster UCDs. To construct the equivalent mass-size relation seen in the right panel of Figure 11, we have estimated the dynamical masses of our UCDs assuming a constant dynamical to stellar mass ratio, calibrated on 18 UCDs that have both literature dynamical masses and stellar masses measured using the approach described in Section 2.7. From these 18 UCDs (spanning the dynamical mass range from 2×10^6 $M_\odot$ to 1.5×10^8 $M_\odot$) we find that the stellar mass of a UCD is 0.54 ± 0.25 times the dynamical mass. With this correction we can estimate the total dynamical masses of our NGC3923 and NGC4546 UCDs. Using these masses, we find that our field/group UCDs conform to the same mass-size trends as cluster UCDs.

As previously noted for Milky Way and Virgo cluster GCs, most GCs display constant size with luminosity or mass (see e.g. Jordán et al. 2005; Rejkuba et al. 2007). In contrast, UCDs exhibit increasing size with luminosity or mass (Haşegan et al. 2005; Evstigneeva et al. 2008; Mieske et al. 2008b). Intriguingly, the most luminous GCs (with $M_V < -10$, or $M > 2 \times 10^6$ $M_\odot$) of Cen A, the Milky Way (ωCen specifically) and M31 also seem to display a luminosity/mass-size trend. The nuclei of dwarf galaxies also display a mass-size trend, with similar slope to that of UCDs, though it appears to be offset to smaller radii (see Figure 11 and Evstigneeva et al. 2008). Like the similarities of these objects in the colour-magnitude diagram, these size trend similarities may be a sign of a comparable formation histories for GCs, UCDs and nuclei, or may merely be due to the influence of the same physical processes (e.g. mass loss by stellar evolution, evaporation and gravitational shocks).

If we use the onset of the luminosity/mass-size trend to classify objects as either GCs or UCDs we determine selection criteria very similar to those found in other studies (e.g. Mieske et al. 2008b). UCD-like behaviour arises at around $M_V = -10$ (masses above 2×10^6 $M_\odot$) and for objects more extended than ~ 6 pc. There is however no clean switch in behaviour at any of these limits. This is clearly demonstrated by the existence of objects (M31 and Cen A GCs, Virgo dwarf nuclei, and Virgo UCDs) that have mass up to 10^7 $M_\odot$ whilst also having half-light radii entirely
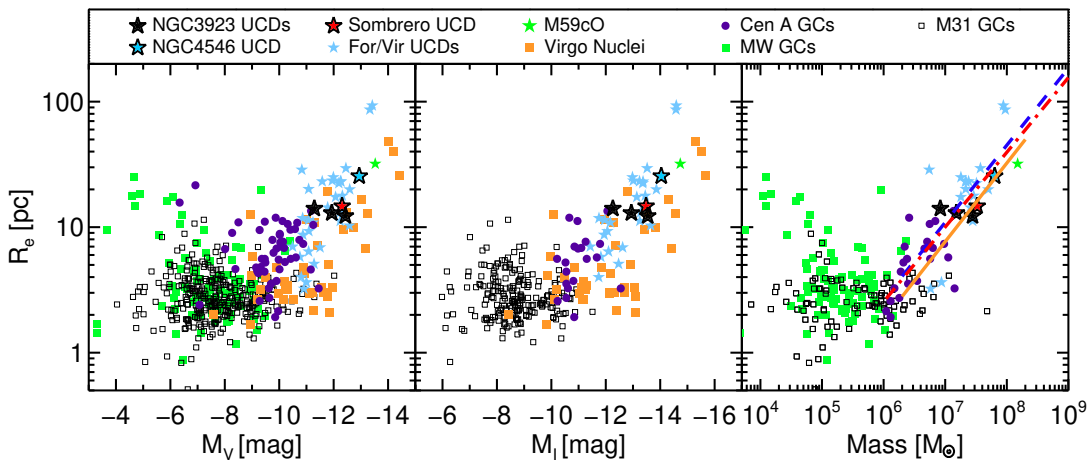
Figure 11. Left and Centre Panels : Half-light radius vs. V/I magnitude for compact stellar systems. Milky Way GCs are from McLaughlin & van der Marel (2005); M31 GCs are from Barmby et al. (2007) and Peacock et al. (2009); Cen A GCs are from Harris et al. (2002), Rejkuba et al. (2007), and Taylor et al. (2010). Fornax and Virgo UCDs are from Evstigneeva et al. (2007b, 2008) and Haşegan et al. (2005). Large stars denote our NGC3923 UCDs, our NGC4546 UCD, and the Sombrero UCD from Hau et al. (2009). The UCD M59cO is from Chilingarian & Mamon (2008). Virgo dwarf nuclei are from Côté et al. (2006) converted to V as described in Section 3.2.2. **Right Panel** : Half-light radius against dynamical mass for GCs/UCDs. Sources as in left panel, except M31 GCs are from Barmby et al. (2007) only and CenA GCs are from Taylor et al. (2010) only. The masses of our NGC3923 and NGC4546 UCDs are estimated dynamical masses, determined as described in Section 3.3.3. The solid orange line is the model prediction of Murray (2009) as described in Section 3.3.3. The dashed blue line is the extrapolation of the relation for bright ellipticals from Haşegan et al. (2005), the red dot-dashed line is the best fit to bright ellipticals, compact ellipticals, and galaxy bulges from Dabringhausen et al. (2008).

consistent with normal GCs. The existence of high-mass objects that do not display a mass-size trend may indicate a second formation channel at work. Regardless, for any sensible GC/UCD separation, our field/group UCDs are all confirmed to be bona-fide UCDs.

The onset of UCD-like behaviour at $M_V \sim -10$ and $R_e > 6$ pc, implies that several nominal GCs previously spectroscopically confirmed to be part of the NGC3923 system by Norris et al. (2008, 2010 in prep.) potentially meet the UCD selection criteria. In fact, examination of the SExtractor CLASS_STAR parameter for spectroscopically confirmed GCs shows that five "GCs" are marginally resolved by the *HST*. However, as the resolution limit of the ACS corresponds to a half-light radius of $\sim$10 pc at the distance of NGC3923, more sophisticated modelling is required to accurately measure the sizes of these objects. At present therefore, we have two confirmed UCDs around NGC3923, one high confidence candidate (UCD3c), and five other probable UCDs. Based on the analysis of spectra in Norris et al. (2008) the stellar populations of these candidate UCDs match those of the exclusively old GCs of NGC3923.

We note with interest that the luminosities where UCD-like luminosity-size behaviour becomes apparent (see Figure 11) correspond well with the luminosities at which the blue tilt of GC systems is strongest (compare Figs. 9 and 11; see also Harris 2009). This apparent concordance perhaps indicates that a common mechanism is responsible for the onset of both mass-size and mass-metallicity relations at an equivalent "scaling onset mass".

The cause of the UCD mass-size trend, and the reason for its sudden onset above $\sim 2 \times 10^6 \, M_\odot$ is still an open question, with several possible solutions, some of which are applicable to multiple of the potential UCD formation channels

(single-cluster GGCs, merged GGCs, and stripped nuclei; see Section 1).

Murray (2009) suggests that single star clusters of mass $> 10^6 \, M_\odot$ are optically thick to far-IR radiation at formation, changing the behaviour of the Jeans mass systematically with cluster mass. This process leads to a top heavy IMF, which can also explain the observation that UCDs have higher mass-to-light ratios than GCs (Chilingarian et al. 2008; Mieske et al. 2008b). The predicted mass-size trend from Murray (2009) is overplotted on Figure 11 as the solid line, providing a good qualitative match to the slope (if not the zeropoint) of the observed mass-size trend. The other predicted behaviours, such as the presence of a top-heavy IMF, and higher mass-to-light ratios provide a useful way to probe the validity of this scenario, and hence, the likely single collapse origin of some UCDs.

Complicating matters however, is the fact that a fit to the scaling relation for bright ellipticals (the dashed line in Figure 11, from Eqn 12. of Haşegan et al. 2005 or the darker dot-dashed line from Dabringhausen et al. 2008) provides an even better fit to the UCD mass-size trend than the Murray (2009) prediction. This observation can itself have two explanations. The first is appropriate for all three possible UCD types (single-cluster GGCs, merged GGCs and dwarf nuclei): as suggested by Mieske et al. (2008b), objects with the size and mass of UCDs (and larger) will be dynamically unrelaxed after a Hubble time, whereas GCs are sufficiently small that they have dynamically relaxed by the present. Recently Gieles et al. (2010) explained this observation in terms of GCs evolving away from a common (with UCDs and elliptical galaxies) mass-size relation due to cluster expansion caused by hard binaries and mass loss in stellar evolution. This scenario does not in itself explain the existence of the mass-size trend, only the reason for GCs' deviation

Name	Distance [kpc]	R_e [pc]	$M_\star$ [$\times 10^6 M_\odot$]	t_{decay} [Gyr]
NGC3923 UCDs				
UCD1	3.23	12.3±0.3 (1.8)	$15.0^{+7.7}_{-7.1}$	7.3
UCD2	7.92	13.0±0.2 (3.2)	$8.2^{+3.1}_{-3.7}$	71.5
UCD3c	6.14	14.1±0.2 (2.3)	$4.5^{+0.9}_{-1.5}$	81.4
NGC4546 UCD				
UCD1	1.16	25.5±(1.3)	$34.3^{+6.9}_{-10.6}$	0.5
Sombrero UCD				
UCD1	7.50	14.7±1.4	$33.0^{+3.0}_{-3.0}$	25.2

Table 4. UCD Structural Properties. Distance is the projected distance between the UCD and galaxy centre. Half-light radii are measured by direct integration of the best-fit GALFIT models as described in Section 2.6.4. Uncertainties without parentheses are based on the measured differences between the half-light radii determined in the F606W and F814W bands; values in parentheses are uncertainties based on the difference between the PSF-convolved and unconvolved estimations. Properties for the Sombrero UCD are from Hau et al. (2009). Computation of UCD masses is described in Sections 2.7 and 3.3.3. The calculation of dynamical friction decay time is described in Section 3.1.

from the trend. Because of this, and because it is applicable to all potential UCD types, it does not provide any useful clues to the formation history of UCDs.

A second explanation for the close correspondence between the mass-size trends of UCDs and elliptical galaxies may be that UCDs form in a manner similar to elliptical galaxies, i.e. by violent relaxation after the merger of sub-components. This explanation could be applicable to GGCs that form on short timescales via the merger of "normal" GCs within a single giant molecular cloud. It may also apply to UCDs formed by the stripping of galaxy nuclei, because one possible formation scenario for galaxy nuclei is that they are built up by the merging of GCs that sink to the centre of their host galaxy by dynamical friction (see e.g. Agarwal & Milosavljevic 2010). In this case, the observation that galaxy nuclei are smaller at fixed mass than UCDs may imply that nuclei that are stripped to become UCDs must expand, e.g. as in Bekki et al. (2003). Since in the merging scenario the existence of the mass-size trend for masses $> 2\times10^6$ M$_\odot$ is directly related to the way in which the objects formed, this scenario is also consistent with the existence of objects with mass $> 2\times10^6$ M$_\odot$ that do not display a mass-size trend, if they did not form by merging.

In each of these scenarios the cause of the common onset for the mass-size and mass-metallicity relations is mysterious. It is of course possible that this close agreement is merely a coincidence, however, any explanation that encompasses both behaviours is to be strongly preferred.

3.4   UCD Frequencies and Environments

In this section we examine whether the numbers and luminosities of our UCDs can be statistically explained as the high luminosity tail of the globular cluster luminosity functions of their host galaxies, arguing that those around NGC3923 and the Sombrero can, while the one near NGC4546 cannot. We also investigate the environmental dependence of UCD frequencies.
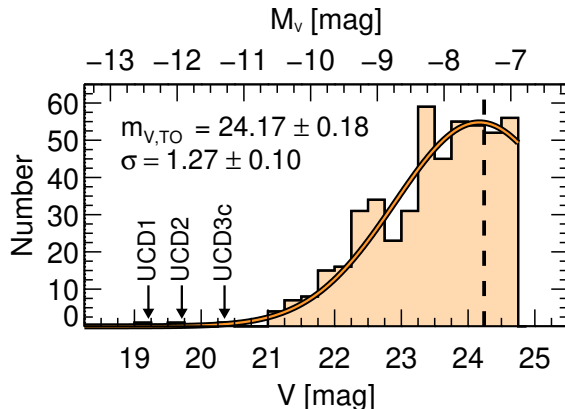

Figure 12. NGC3923 V-band GC luminosity function. The best-fit Gaussian model is overplotted with the best-fit parameters listed in the top left. Assuming the Table 1 distance modulus of 31.64, the measured turnover magnitude equates to an absolute magnitude of $M_V = -7.47$, consistent with the observed universal GCLF turnover magnitude of $\sim -7.4 \pm 0.1$ shown by the dashed line (e.g. Kundu & Whitmore 2001a,b; Jordán et al. 2007).

3.4.1   GCLF Analysis

Hilker (2009a) demonstrates that in most cases the absolute magnitude of the brightest GC/UCD of a galaxy correlates with the host galaxy luminosity and the total GC system size. Furthermore, he shows that the absolute magnitude of a galaxy of the brightest GC/UCD is well fit by a simple model where the observed GCLF is extrapolated to higher luminosities. This result implies that UCDs are in general the extreme high luminosity tail of the GC luminosity function. One natural result of such a scenario is that galaxies are often expected to host multiple UCDs, if their GC systems are large enough. The fact that we have discovered at least two, and as many as eight UCDs associated with NGC3923, would seem to lend support to their having been formed alongside the GCs of NGC3923. It is difficult to imagine that stripping of nuclei could produce so many similar, massive objects with long-lived orbits.

We wish to determine whether our field/group UCDs obey the Hilker (2009a) correlations. Where possible we make use of literature determinations of the GCLF parameters; for the Sombrero we use the GCLF total size and dispersion measured by Rhode & Zepf (2004). Unfortunately, no suitable imaging data exists to allow an analysis of the GCLF of NGC4546. In the case of NGC3923 we use the determination of the total GC system size made by Sikkema et al. (2006), but unfortunately neither Sikkema et al. (2006) nor Cho (2008) quote the dispersion of the GCLF of NGC3923 needed to predict the brightest GC/UCD. We have therefore examined the *HST* photometry described in Section 2.6.3 to determine the dispersion of the NGC3923 GCLF. Full details of the procedure used to determine this are provided in Appendix B, see also Figure 12.

The left panel of Figure 13 shows the result of placing our field/group UCDs on the brightest GC/UCD vs. host galaxy luminosity plot. The UCDs of NGC3923 and the Sombrero are perfectly consistent with the overall trend of more luminous galaxies having more luminous brightest
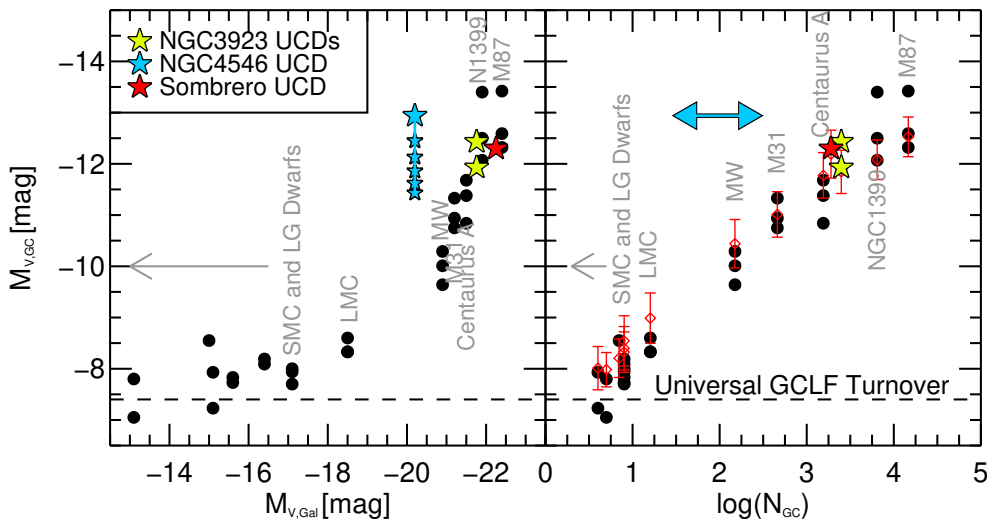
Figure 13. Figure after Hilker (2009a). **Left Panel** : The absolute magnitude of the brightest two or three GCs/UCDs of a galaxy as a function of host galaxy total luminosity. Data come from the compilation of Hilker (2009a) plus estimates for NGC3923, NGC4546 and the Sombrero as described Section 3.4.1. The smaller blue stars are predictions for the future evolution of NGC4546 UCD1 for ages (top to bottom) 5, 7, 9, 11 and 13 Gyr. **Right Panel** : The absolute magnitude of the brightest two or three GCs/UCDs of a galaxy as a function of the total number of GCs present in the GC system of the host galaxy. The red diamonds with error bars indicate the average luminosity of the brightest GC found in 10,000 Monte-Carlo simulations of the GCLF of each galaxy, assuming the measured total number of clusters, the universal GCLF turnover and the measured dispersion of the GCLF. The blue arrowed region shows where NGC4546 UCD1 is likely to lie in this plot.

GC/UCDs. However, the NGC4546 UCD is substantially overluminous relative to this trend, being around 3 magnitudes brighter than expected given the low luminosity of NGC4546. Even if we artificially evolve the NGC4546 UCD forward in age using the models of Maraston (2005) to ages 5, 7, 9, 11 and 13 Gyr (top to bottom small blue stars in Figure 13), the NGC4546 UCD will still be significantly overluminous relative to its host galaxy.

The right panel of Figure 13 demonstrates that the magnitudes of the UCDs of NGC3923 and the Sombrero correlate extremely well with total GC system size, again confirming Hilker's result. Despite the fact that we cannot presently place the NGC4546 UCD on this plot, we can still state with some certainty that this UCD cannot be explained as bright extension of the GCLF. The horizontal arrow marks M_V for this UCD in the plot, showing that empirically it could occur in galaxies with GC systems as large as those in M87. However, for a galaxy of NGC4546's modest luminosity to produce such a large GC would require either the most unlikely statistical fluke, or that NGC4546 has a most unusual GC system, being extremely large for its host mass. Moreover, we suspect that the brightest UCDs around NGC1399 and M87 cannot be formed as GCs, based on statistical arguments. Further support for the idea that the brightest NGC1399 and M87 UCDs are in fact stripped nuclei comes from the presence around both of extended low surface brightness envelopes (Evstigneeva et al. 2008), of the sort expected to persist after stripping.

The red diamonds in Figure 13 show predictions of a model in which two effects conspire to determine the expected magnitude of the brightest GC/UCD of a galaxy. The first is simply the increasing number of GCs found in larger galaxies. The second, more subtle effect, is that the dispersion of the GCLF of a galaxy depends on galaxy lu-

minosity/mass (Jordán et al. 2007), such that more luminous galaxies have broader GCLFs, making higher luminosity GCs more likely.

Our model estimates the *expected* magnitude of the brightest GC/UCD of an observed GC system, as equal to the average magnitude of the brightest GC found in 10,000 Monte-Carlo simulations using the observed total GC system size, observed GCLF dispersion, and an assumed universal GCLF turnover magnitude of $M_V = -7.4$. As found by Hilker (2009a) the predictions of this simple model are remarkably close to those found for galaxies from dwarfs to BCGs. The only exceptions appear to be the brightest UCDs of the NGC1399 and M87 systems. These objects are too luminous to be explained as an extension of the GCLF of NGC1399 or M87. For these UCDs to be luminous GCs would require that either: the total number of GCs present in the M87 and NGC1399 systems is currently underestimated by greater than a factor of 5, or, the dispersion of the GCLF of these galaxies is underestimated by ∼25%.

We consider errors of this size unlikely, and therefore suggest *that M_V of around –13 represents the practical upper magnitude limit for the existence of UCDs formed as GGCs.* GC systems of the required richness to produce larger UCDs aren't yet known, even relying only on statistical arguments and without bringing up physical objections to producing the large giant molecular clouds required. Above this limit UCDs are likely to be the result of other processes, such as the stripping of galaxy nuclei, while below this limit either process could be responsible, but GC-like formation seems most common, given the typically close correspondence between GC numbers and GC/UCD maximum luminosity.

3.4.2 *UCD Environmental Dependence*

Our discovery of at least three further UCDs in non-cluster environments takes the number of UCDs found outside of high-density environments to five. Clearly UCDs are not simply a high density environment phenomenon. In fact, as Figure 14 demonstrates, UCDs are found everywhere from galaxy clusters such as Virgo and Fornax, through groups such as the NGC3923 group, to loose group/isolated galaxies such as NGC4546 and the Sombrero. This observation does not itself rule out any of the UCD formation scenarios, as all possible formation routes are expected to occur in all environments, though with varying levels of efficiency.

Within the limits of present samples, it is not yet possible to draw firm conclusions about the environmental distribution of UCDs, as much larger and more carefully constructed samples making use of wider field HST imaging (for accurate GC/UCD separation) than available presently would be required for that. However, the number of UCDs found by our mini survey is in line with previous estimates of UCD frequency in clusters. Given that the ACS field of view covers an area of 0.003 deg^2 and that the WFPC2 covers 0.001 deg^2, we can use the distances to each of our 76 examined galaxies to estimate the area probed. In total we find that we have examined 0.022 Mpc^2. If we make the assumption that UCDs are as common in all environments as in the Fornax cluster (105±13 per circle of radius 0.9°, Gregg et al. 2009), then there should be 375 UCDs/Mpc^2. Therefore, given the area surveyed we would expect to find 9 UCDs, a number in good agreement with our 11 candidates (4 spectroscopically confirmed). If we also consider that the number of UCDs found by Gregg et al. (2009) undoubtedly includes some interloping intracluster GCs (as Gregg et al. 2009 lack the high resolution imaging required to measure radii), then even without any further UCD candidates being confirmed, the number of UCDs in field/group environments appears similar to the number in galaxy clusters.

4   DISCUSSION

The preceding sections have presented multiple properties of a sample of confirmed field/group environment UCDs. We now synthesise the implications of these observations for the formation of these UCDs in particular, as well as the formation of UCDs and GCs in general.

4.1   Individual Cases

NGC4546 UCD1: The results of our investigation suggest that NGC4546 UCD1 is the first unambiguous example of a UCD formed through the stripping of a companion galaxy. Direct evidence includes the young measured age of NGC4546 UCD1, an age inconsistent with those determined for the vast majority of GCs and UCDs to date. If this UCD had formed through GC formation processes, we would expect to see a similarly young GC population, formed alongside the UCD. Although our imaging is relatively shallow, we see no clear evidence for a population of bright (young) GCs associated with NGC4546. It would also seem extremely unlikely that NGC4546 could undergo a recent bout of star and cluster formation, whilst displaying

the observed universally old ages for the diffuse light of the galaxy. The observed [α/Fe] of ~0.0 for NGC4546 UCD1 is also interesting, implying a more prolonged period of star formation than typical for GCs, which generally have super-solar α/Fe (e.g. Puzia et al. 2005; Norris et al. 2008).

The conclusion that NGC4546 UCD1 is not associated with GC formation processes is additionally supported by the observation that the UCD is significantly overluminous relative to the luminosity of the host galaxy (see Figure 13). This UCD will remain overluminous even when observed at 13 Gyr old, meaning that even if it is a recently formed GGC, it is still extremely difficult to explain statistically as a bright outlier of the GCLF. However, it is unlikely to survive as long as 13 Gyr, as its calculated dynamical friction timescale is of the order of 0.5 Gyr, consistent with a relatively recently formed and short lived object.

Additional evidence for the stripped minor companion origin of the NGC4546 UCD is provided by the fact that NGC4546 itself has significant quantities of counterrotating gas (Galletta 1987; Sage & Galletta 1994; Sarzi et al. 2006). This gas rotates in the *same* direction as the UCD but in the opposite direction and slightly out of plane relative to the stellar disc of NGC4546. It therefore seems highly likely that NGC4546 UCD1 is the remaining nucleus of a galaxy stripped within the last few Gyr by NGC4546.

It is possible to estimate the mass of the galaxy that was stripped to form the UCD of NGC4546 using the observed relation between the nuclear mass of a galaxy (nuclear star cluster + supermassive black hole) and the mass of the galaxy spheroid (Graham & Spitler 2009). By combining Graham & Spitler's Eqn. 2 with the measured UCD mass (from our Table 4), and assuming that the mass of the supermassive black hole of the progenitor was negligible relative to the mass of the nuclear star cluster, we find that the spheroid of the progenitor had a stellar mass of ~$3.4^{+1.2}_{-1.5} \times 10^9$ M$_\odot$. This estimate neglects the gaseous component of the progenitor, for which we can set a lower limit from the current mass of counterrotating gas (assumed to come entirely from the progenitor): $M_{HI} = 1.2 \times 10^8$ M$_\odot$ (Bettoni et al. 1991) and $M_{H_2} = 9.6 \times 10^7$ M$_\odot$ (Sage & Galletta 1994). Based on typical gas fractions at the progenitor stellar mass (e.g. Wei et al. 2010), we suspect that the progenitor originally had much more gas than remains in cold form.

The estimated progenitor mass is intriguing for two reasons. For one, it is approximately a factor of ten less than that of NGC4546 (M ≈ 3×10^{10} M$_\odot$, Table 1), which would allow NGC4546 to disrupt the smaller galaxy without being significantly disordered itself — reassuring as NGC4546 appears undisturbed. The progenitor mass estimate is also interesting because it lies very near the transition between dwarf and giant galaxies (the "threshold mass" discussed in Section 3.2.2 and Kannappan et al. 2009). This result is important because as Figure 9 demonstrates, if it lived long enough, the NGC4546 UCD would eventually redden and fade to take up a position in the colour-magnitude diagram consistent with the nuclei of giant galaxies. The UCD only lies on the blue colour-magnitude locus currently because it is young. Thus the progenitor seems to have had just enough mass to generate a metal-rich nucleus, but not enough that a large spheroid or more violent merger would have been expected.
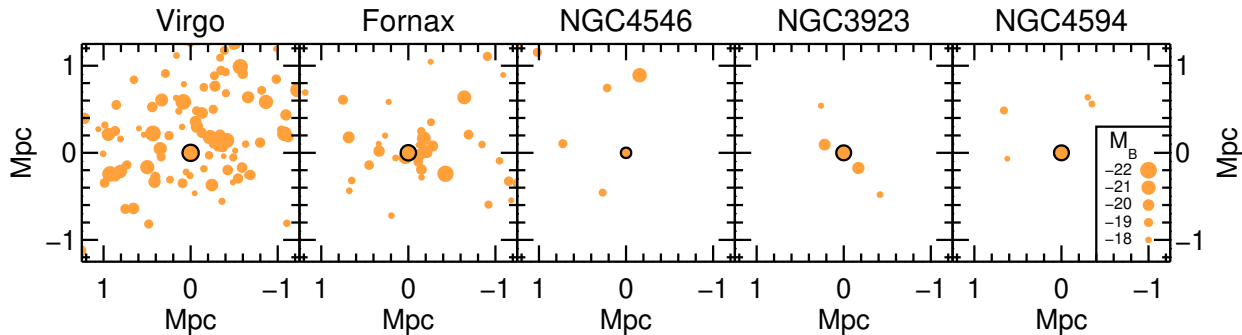
Figure 14. Illustration of the relative environmental densities of the galaxies studied here. The equivalent panels for the Virgo and Fornax clusters are provided to facilitate comparison with the denser environments where UCDs are generally studied. In each panel filled dots indicate galaxies found to be members of the same structure as the galaxy of interest by Giuricin et al. (2000), where we apply a magnitude cut at $M_B < -17.65$ (the magnitude limit at the distance of the most distant group, NGC3923 and coincidentally similar to the dwarf-giant luminosity division discussed in Section 3.2.2). The size of the filled dots is proportional to the M_B of each galaxy. The central galaxies hosting UCDs are indicated by black circles (M87, NGC1399, NGC3923, NGC4546 and the Sombrero respectively).

NGC3923 UCDs: A wealth of circumstantial evidence points to the conclusion that the NGC3923 UCDs are GGCs. The existence of multiple UCDs with similar properties (e.g. size) would seem unlikely if they were to be the result of several minor merger events. Moreover we appear to see the beginnings of transition objects, in the form of five GCs spectroscopically confirmed by Norris et al. (2008, 2010, in prep.), which have luminosities and likely radii that place them between the ∼3 pc GCs and the ∼13 pc UCDs of NGC3923. This behaviour is very similar to that seen by Taylor et al. (2010) for the more massive GCs of CenA, which similarly appear to bridge the gap between GCs and UCDs. Also interesting is the fact that three of the five transitional GCs in NGC3923 have measured stellar populations (from Norris et al. 2008) that place them squarely in the normal GC regime. They are all old (age greater than 12 Gyr), with intermediate to high metallicity ([Z/H] from –0.4 to 0.2), and supersolar [α/Fe]. Although direct stellar population measurements are not yet available for the UCDs, evidence of a close connection between the UCDs and GCs of NGC3923 is provided by the fact that the UCDs smoothly extend the observed blue tilt in the colour-magnitude relation of the blue GCs, suggesting a common mass-metallicity relation.

A GGC origin for the NGC3923 UCDs is also consistent with the computed dynamical friction decay timescales. These are all long ($t_{decay} > 7$ Gyr), implying that the UCDs could be as long lived as the GCs of NGC3923, which have ages > 10 Gyr (Norris et al. 2008). A final persuasive piece of evidence for a connection between the GCs and UCDs of NGC3923 is provided by the fact that the UCDs are statistically consistent with being the luminous extension of the observed GC luminosity function.

Sombrero UCD: As discussed in Hau et al. (2009) the Sombrero UCD is old (12.6 Gyr), metal rich ([Fe/H] = –0.08), and has a slightly supersolar alpha-element enhancement ([α/Fe] = 0.06). These stellar population parameters are consistent with those determined for members of the GC population of the Sombrero by Larsen et al. (2002), as well as being close to that measured for the centre of the Sombrero itself by Sánchez-Blázquez et al. (2006). Its

calculated dynamical friction timescale is also long (longer than a Hubble time), indicating it is likely a long lived object. When combined with the fact that this UCD can be explained statistically as the massive limit of the Sombrero GC system (see Figure 13), it would seem most likely that this UCD has a GGC origin. The fact that there are currently no known objects with luminosities between that of the UCD and the most luminous GCs of the Sombrero may simply reflect the relatively incomplete nature of the spectroscopic coverage of the Sombrero GC system (Hau, private communication). However, despite the compelling circumstantial evidence it is impossible to be certain that this UCD is a GGC. In particular, this UCD could be the result of the stripping of a late-type companion galaxy, if the stripping occurred early in the lifetime of the Sombrero on an orbit that allowed the nucleus survive unusually long. It could also be the result of the stripping of an early-type dwarf with an older nucleus in the more recent past, a plausible scenario given that the Sombrero is known to have some apparently tidal features (Malin & Hadley 1997). Possible direct evidence for a stripping origin for the Sombrero UCD is provided by the fact that the generalised King, King, and Sersic models for this UCD all show leftover low surface brightness features, components that are not seen in the other UCDs (see Figure 10).

4.2 Integrating UCD and GC Formation

Overall, our observations support the idea that UCDs are a "mixed bag" of objects (Hilker 2009b; Taylor et al. 2010; Da Rocha et al. 2010), composed of GGCs and stripped nuclei. We are also confident that the GC systems of galaxies are themselves mixed bags, composed of several types of object with different formation histories: 1) normal GCs formed in situ, i.e. formed in the galaxies in which they currently reside by any of the proposed GC formation scenarios such as dissipational collapse (Forbes et al. 1997) or merger induced star formation (Ashman & Zepf 1992); 2) GCs accreted from smaller companions; 3) a population of lower mass stripped dwarf nuclei. In Figures 15 and 16 we present an illustration of a possible GC, UCD, and nucleus formation scheme consistent with this interpretation.

In our proposed scenario, "normal" GCs form as single collapse clusters, while some, perhaps most, UCDs form alongside their host galaxy GC system as GGCs. The GGC-type UCDs are differentiated observationally from GCs by the onset of a mass-size trend for cluster mass greater than the scaling onset mass of 2×10^6 M$_\odot$ (the same break point found in the mass-size relation by e.g. Haşegan et al. 2005; Mieske et al. 2008b; Taylor et al. 2010). The observed change in mass-size behaviour between GC and GGC is either the result of a change in the opacity of star forming regions at the scaling onset mass (e.g. Murray 2009, and Section 3.3.3), or the result of hierarchical merging of multiple YMCs within a single star forming complex. In either of these cases the stellar populations of the resulting GGC-type UCDs would largely indistinguishable from those of other lower mass normal GCs that escaped from the same star forming complexes without merging. In particular, even for UCDs formed by merging, the timescale of star formation and merging for each UCD should be relatively rapid ($<$ a few hundred Myr). Such a short star forming epoch leads to supersolar alpha-element enhancement, as is usually found in normal GCs (e.g. Puzia et al. 2005; Norris et al. 2008).

How far this hierarchical process may proceed is uncertain; building the most massive UCDs would likely require the merger of hundreds of normal GCs, a process that seems somewhat implausible. This would therefore seem to imply the existence of an upper limit to the size of the UCDs that this process could create, at least in practice. From purely statistical arguments (see Section 3.4.1), and assuming the number of merged systems scales as the number of unmerged GCs, we suggest that 7×10^7 M$_\odot$ (M$_V$ = –13 for old systems) represents the practical upper limit to UCD formation by GC-like processes. GC systems sufficiently rich to populate above this limit (either by merging GCs or by the collapse of single giant clouds with changed physics) are not known at the present time. We note that our suggested upper limit of 7×10^7 M$_\odot$ is also very similar to the mass of stars formed in superclusters (clusters of star clusters) seen in some interacting and strongly star forming galaxies. Fellhauer & Kroupa (2005) model the evolution of such structures and find that they can indeed merge over short ($<$ a few hundred Myr) timescales to form UCD-like objects such as the young ($\sim$500 Myr), massive (dynamical mass $\sim$ 8×10^7 M$_\odot$) cluster W3 associated with the merger remnant NGC7252 (Maraston et al. 2004).

On top of this population of GCs and GGC-type UCDs intrinsic to the host galaxy, there are two sets of interloper stellar systems. The first is simply the population of normal GCs provided to larger galaxies by accreted galaxies (these are mostly blue GCs, as low mass galaxies have very few red GCs, e.g., Lotz et al. 2004; Peng et al. 2006). This population can be a significant fraction of a galaxy's GC system. Recent work on the Milky Way GC system shows that perhaps 25% of its GCs could have been provided by 6-8 dwarf galaxies (Forbes & Bridges 2010). Similarly Mackey et al. (2010) find that $\gtrsim$80% of Andromeda's outer GCs are likely to have been accreted from dwarf satellites.

The second (presumably smaller) population of interlopers is provided by the nuclei of the accreted galaxies. If a stripped nucleus has M $<$ 2×10^6 M$_\odot$ (and has a small radius), it is possible for it to be lost amongst the larger population of normal GCs, at least in colour-magnitude and mass-size space. In principle an in-depth examination of the object's stellar populations may provide clues to its true origin, especially if its [α/Fe] ratio is depressed relative to GCs, as galaxy nuclei are expected to have longer formation timescales than GCs/GGCs. It has been suggested that such remnant nuclei include ω Centauri in the Milky Way (e.g. Hilker & Richtler 2000; Mackey & van den Bergh 2005) and G1 around the Andromeda galaxy (e.g. Meylan et al. 2001). Alternatively, if the remnant nucleus has M $>$ 2×10^6 M$_\odot$ it will be classified as a UCD. The UCD of NGC4546 is the first conclusive example of such a stripped-nucleus UCD.

Such stripped-nucleus UCDs can also explain the existence of UCDs above the apparent upper magnitude limit for GGC-type UCDs at M$_V$ $\sim$ –13. Interestingly, examination of Figure 9 demonstrates that for these most extreme objects, it is not in fact dwarf galaxies (M$_B$ $>$ –17.6, V$_{circ}$ $<$ 120 kms^{-1}) that must be stripped, but likely giant galaxies (though perhaps "small giants" as in the NGC4546 case; see Section 4.1). As well as being consistent with the most luminous UCDs, the galaxy nuclei observed in group/cluster samples have the correct colour-magnitude trends to explain any blue GC/UCD as well as the more luminous red UCDs. At first glance it would seem that red objects with M$_V$ fainter than $\sim$–11 (the magnitude of the lowest luminosity red nuclei in Figure 9) must form only through GC-like processes. However, it is possible that red nuclei (from giant galaxies), or massive blue nuclei with colours as red as low-mass red GCs (from relatively high mass dwarf galaxies), may lose much of their mass during the stripping event and during their subsequent dynamical evolution in the larger galaxy potential. This stripping/disruption could allow objects that started out with M$_V$ more luminous than –11 to eventually fade into the lower luminosity region mostly inhabited by red GGCs.

5   CONCLUSIONS

Using SOAR/Goodman imaging and spectroscopy, SAURON IFU spectroscopy, and archival *HST* ACS and WFPC2 imaging, we have investigated a sample of field/group UCDs. Our main conclusions are as follows:

• To first order we find that low density environment UCDs are as common as UCDs in galaxy clusters.
• Combining our UCD sample with literature data we confirm that UCDs are a "mixed bag" (Hilker 2009b; Taylor et al. 2010; Da Rocha et al. 2010), composed of objects we term giant-GCs (GGCs), and stripped galaxy nuclei.
• In the NGC4546 UCD we find the first unambiguous example of a young UCD formed by the stripping of a galaxy nucleus. The UCD of NGC4546 is young ($\sim$3.4 Gyr), metal rich, and has near solar alpha-element abundance ratios. In stark contrast the diffuse light of NGC4546 is old ($\sim$10 Gyr), intermediate in metallicity, and has supersolar [α/Fe]. Additionally the NGC4546 UCD is significantly overluminous relative to the host galaxy, and hence cannot be explained as the bright extension of the GCLF of NGC4546. The short dynamical friction decay timescale of 0.5 Gyr of this UCD also indicates that it is likely a short lived object.
• We have discovered multiple UCDs (at least two, possibly as many as eight) associated with the group shell el-
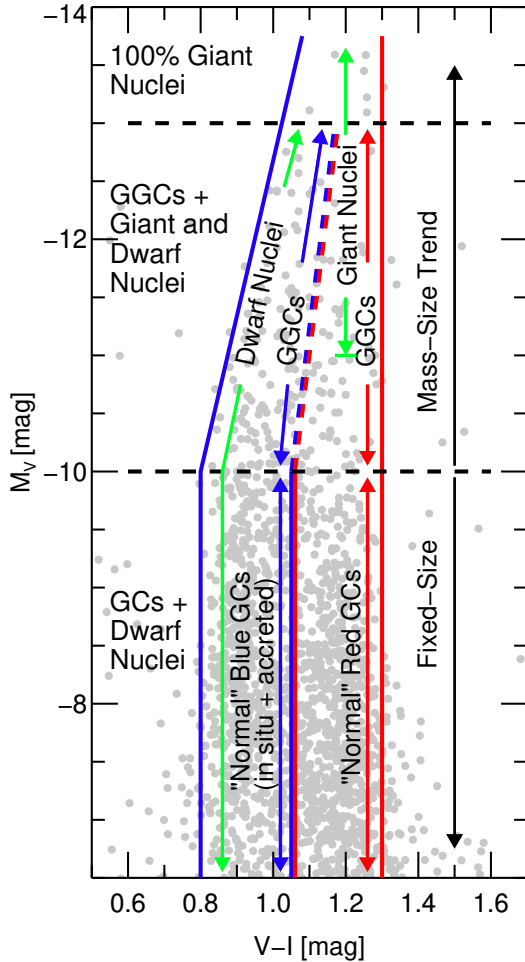
Figure 15. Illustration of a possible scheme describing the origin of GCs and UCDs. The light grey circles are all GCs, UCDs and dwarf nuclei presented in Figure 9. "Normal" GCs refers to those GCs that formed from the collapse of a single giant molecular cloud, and that display a fixed radius with mass trend (i.e. have $M < 2 \times 10^6$ M$_\odot$). UCDs are divided into two subgroups, those that form in a GC type manner (i.e. from giant molecular clouds that may or may not merge), which we call GGCs, and those that are the result of stripping the nucleus from a galaxy. Depending on the luminosity of the accreted nucleus, it could be classed as a UCD or mistaken for a normal (usually blue) GC. The black dashed line at $M_V = -10$ indicates the approximate location of the "scaling onset luminosity", the black dashed line at $M_V = -13$ indicates the luminosity above which UCDs are expected to be exclusively stripped nuclei. The dashed red and blue lines indicate the uncertain division between red and blue GCs/UCDs/nuclei at higher luminosities, due to the increasing effects of self-enrichment on the colours of "blue" GCs/UCDs/nuclei.

Figure 16. Cartoon schematic showing the origin of various objects in the mass-size plane. UCDs are divided into GGCs, formed either singly or through merging, and stripped galaxy nuclei. Those GCs appearing as "normal" GCs (either formed in situ or accreted) are contaminated by lower mass stripped galaxy nuclei.

GCLF of the Sombrero. Additionally it has a long dynamical friction decay timescale (> 25 Gyr).

• We find that the colour-magnitude diagrams of dwarf nuclei, blue GCs, and blue UCDs are indistinguishable. Dwarf nuclei exist over the entire range of blue GC and UCD luminosities. All three populations display the same "blue tilt" phenomenon (a mass-metallicity relation). Red GCs, red UCDs, and more massive dwarf/giant galaxy nuclei also show considerable overlap in colour-magnitude space but display no evidence for a mass-metallicity relation.

• We suggest the existence of a common "scaling onset mass" of $\sim$2$\times$10^6 M$_\odot$ marking the onset of both a mass-size relation (defining UCDs as a class) and a mass-metallicity relation (the blue tilt). In line with previous studies we find that UCDs (of either GGC or stripped nucleus type) may be efficiently selected by requiring objects to have $R_e > 6$ pc and $M_V < -10$ or mass $> 2\times10^6$ M$_\odot$.

• From statistical arguments we suggest $M_V < -13$ as the upper luminosity limit for an old UCD formed via the GGC route. GC systems sufficiently populous to create GGCs above this limit do not exist at the present epoch.

• We present a general scheme that unifies the formation of GCs, UCDs (both GGCs and stripped nuclei), and galaxy nuclei. We argue that the evidence points to a scenario in which the UCDs of NGC3923 and perhaps the majority of UCDs in general are GGCs. These GGCs form alongside normal GCs (perhaps even from the merging of normal GCs) during the major epochs of spheroid assembly. Superimposed on this population is a second population of UCDs produced by the stripping of nuclei from galaxies. These objects are most easily identified in cases where the resulting UCD is too luminous to be explained as the bright end of the GCLF (as in the case of the NGC4546 UCD, Fornax UCD3, and Virgo VUCD7). Such objects could also occur at fainter magnitudes, hidden by the indistinguishable colours of blue GCs/UCDs and dwarf nuclei.

liptical NGC3923. This multiplicity of UCDs, along with the fact that the UCDs all have long dynamical friction decay timescales, and that they are consistent with the extrapolation of the GCLF and colour-magnitude diagram of NGC3923, indicates that these UCDs are GGCs.

• The UCD of the Sombrero galaxy is likely a GGC but a stripping origin cannot be ruled out. Its stellar populations are consistent with those of the GC system of the Sombrero, and its luminosity is explainable as the bright end of the

The existence of two populations of Ultra Compact Dwarfs, one related to the major epochs of spheroid assembly and one to minor merger events, is clearly of great utility in the study of galaxy formation. In order for UCDs to fullfill their potential as probes of the galaxy formation process, it will be necessary to be able to more cleanly separate the two distinct UCD types from each other. To help achieve this goal we are now undertaking a comprehensive survey of all available *HST* imaging and following up with spectroscopy to find UCDs located in all environments. This large sample will allow us to examine the demographics of each UCD type and probe the implications for minor and major merger rates as a function of environment.

6   ACKNOWLEDGEMENTS

REFERENCES

Agarwal M., Milosavljevic M., 2010, ArXiv e-prints

Ashman K. M., Bird C. M., Zepf S. E., 1994a, AJ, 108, 2348

—, 1994b, AJ, 108, 2348

Ashman K. M., Zepf S. E., 1992, ApJ, 384, 50

Bacon R., Copin Y., Monnet G., Miller B. W., Allington-Smith J. R., Bureau M., Carollo C. M., Davies R. L., Emsellem E., Kuntschner H., Peletier R. F., Verolme E. K., de Zeeuw P. T., 2001, MNRAS, 326, 23

Bailin J., Harris W. E., 2009, ApJ, 695, 1082

Barmby P., McLaughlin D. E., Harris W. E., Harris G. L. H., Forbes D. A., 2007, AJ, 133, 2764

Bekki K., Couch W. J., Drinkwater M. J., 2001, ApJ, 552, L105

Bekki K., Couch W. J., Drinkwater M. J., Shioya Y., 2003, MNRAS, 344, 399

Bekki K., Freeman K. C., 2003, MNRAS, 346, L11

Bell E. F., de Jong R. S., 2001, ApJ, 550, 212

Bertin E., Arnouts S., 1996, A&AS, 117, 393

Bettoni D., Galletta G., Oosterloo T., 1991, MNRAS, 248, 544

Binney J., Tremaine S., 2008, Galactic Dynamics: Second Edition, Binney, J. & Tremaine, S., ed. Princeton University Press

Brown R. J. N., Forbes D. A., Silva D., Helsdon S. F., Ponman T. J., Hau G. K. T., Brodie J. P., Goudfrooij P., Bothun G., 2003, MNRAS, 341, 747

Bruzual G., Charlot S., 2003, MNRAS, 344, 1000

Cappellari M., Emsellem E., 2004, PASP, 116, 138

Chilingarian I., Mieske S., Hilker M., Infante L., 2010, ArXiv e-prints

Chilingarian I. V., Cayatte V., Bergond G., 2008, MNRAS, 390, 906

Chilingarian I. V., Mamon G. A., 2008, MNRAS, 385, L83

Cho J., 2008, PhD thesis, University of Durham

Clemens J. C., Crain J. A., Anderson R., 2004, in Society of Photo-Optical Instrumentation Engineers (SPIE) Conference Series, Vol. 5492, Society of Photo-Optical Instrumentation Engineers (SPIE) Conference Series, A. F. M. Moorwood & M. Iye, ed., pp. 331–340

Côté P., Piatek S., Ferrarese L., Jordán A., Merritt D., Peng E. W., Haşegan M., Blakeslee J. P., Mei S., West M. J., Milosavljević M., Tonry J. L., 2006, ApJS, 165, 57

Da Rocha C., Mieske S., Georgiev I. Y., Hilker M., Ziegler B. L., Mendes de Oliveira C., 2010, ArXiv e-prints

Dabringhausen J., Hilker M., Kroupa P., 2008, MNRAS, 386, 864

Dalcanton J. J., Yoachim P., Bernstein R. A., 2004, ApJ, 608, 189

Drinkwater M. J., Jones J. B., Gregg M. D., Phillipps S., 2000, Publications of the Astronomical Society of Australia, 17, 227

Elson R. A. W., 1999, in Globular Clusters, C. Martínez Roger, I. Perez Fournón, & F. Sánchez , ed., pp. 209–248

Evstigneeva E. A., Drinkwater M. J., Jurek R., Firth P., Jones J. B., Gregg M. D., Phillipps S., 2007a, MNRAS, 378, 1036

Evstigneeva E. A., Drinkwater M. J., Peng C. Y., Hilker M., De Propris R., Jones J. B., Phillipps S., Gregg M. D., Karick A. M., 2008, AJ, 136, 461

Evstigneeva E. A., Gregg M. D., Drinkwater M. J., Hilker M., 2007b, AJ, 133, 1722

Fellhauer M., Kroupa P., 2002, MNRAS, 330, 642

—, 2005, MNRAS, 359, 223

Firth P., Drinkwater M. J., Evstigneeva E. A., Gregg M. D.,

Karick A. M., Jones J. B., Phillipps S., 2007, MNRAS, 382, 1342

Firth P., Drinkwater M. J., Karick A. M., 2008, MNRAS, 389, 1539

Forbes D. A., Bridges T., 2010, MNRAS, 404, 1203

Forbes D. A., Brodie J. P., Grillmair C. J., 1997, AJ, 113, 1652

Forbes D. A., Spitler L. R., Harris W. E., Bailin J., Strader J., Brodie J. P., Larsen S. S., 2010, MNRAS, 403, 429

Galletta G., 1987, ApJ, 318, 531

Garnett D. R., 2002, ApJ, 581, 1019

Gieles M., Baumgardt H., Heggie D., Lamers H., 2010, ArXiv e-prints

Giuricin G., Marinoni C., Ceriani L., Pisani A., 2000, ApJ, 543, 178

Goerdt T., Moore B., Kazantzidis S., Kaufmann T., Macciò A. V., Stadel J., 2008, MNRAS, 385, 2136

Graham A. W., Spitler L. R., 2009, MNRAS, 397, 2148

Gregg M. D., Drinkwater M. J., Evstigneeva E., Jurek R., Karick A. M., Phillipps S., Bridges T., Jones J. B., Bekki K., Couch W. J., 2009, AJ, 137, 498

Haşegan M., Jordán A., Côté P., Djorgovski S. G., McLaughlin D. E., Blakeslee J. P., Mei S., West M. J., Peng E. W., Ferrarese L., Milosavljević M., Tonry J. L., Merritt D., 2005, ApJ, 627, 203

Harris W. E., 2009, ApJ, 699, 254

Harris W. E., Harris G. L. H., Holland S. T., McLaughlin D. E., 2002, AJ, 124, 1435

Harris W. E., Whitmore B. C., Karakla D., Okoń W., Baum W. A., Hanes D. A., Kavelaars J. J., 2006, ApJ, 636, 90

Hau G. K. T., Spitler L. R., Forbes D. A., Proctor R. N., Strader J., Mendel J. T., Brodie J. P., Harris W. E., 2009, MNRAS, 394, L97

Hilker M., 2009a, ArXiv e-prints:0906.0776

—, 2009b, UCDs - A Mixed Bag of Objects, Richtler, T. & Larsen, S., ed., pp. 51–+

Hilker M., Infante L., Vieira G., Kissler-Patig M., Richtler T., 1999, A&AS, 134, 75

Hilker M., Richtler T., 2000, A&A, 362, 895

Jensen J. B., Tonry J. L., Barris B. J., Thompson R. I., Liu M. C., Rieke M. J., Ajhar E. A., Blakeslee J. P., 2003, ApJ, 583, 712

Jones J. B., Drinkwater M. J., Jurek R., Phillipps S., Gregg M. D., Bekki K., Couch W. J., Karick A., Parker Q. A., Smith R. M., 2006, AJ, 131, 312

Jordán A., Côté P., Blakeslee J. P., Ferrarese L., McLaughlin D. E., Mei S., Peng E. W., Tonry J. L., Merritt D., Milosavljević M., Sarazin C. L., Sivakoff G. R., West M. J., 2005, ApJ, 634, 1002

Jordán A., McLaughlin D. E., Côté P., Ferrarese L., Peng E. W., Mei S., Villegas D., Merritt D., Tonry J. L., West M. J., 2007, ApJS, 171, 101

Kannappan S. J., 2004, ApJ, 611, L89

Kannappan S. J., Fabricant D. G., Franx M., 2002, AJ, 123, 2358

Kannappan S. J., Gawiser E., 2007, ApJ, 657, L5

Kannappan S. J., Guie J. M., Baker A. J., 2009, AJ, 138, 579

Kannappan S. J., Wei L. H., 2008, in American Institute of Physics Conference Series, Vol. 1035, The Evolution of Galaxies Through the Neutral Hydrogen Window,

R. Minchin & E. Momjian, ed., pp. 163–168

King I., 1962, AJ, 67, 471

Krist J., 1995, in Astronomical Society of the Pacific Conference Series, Vol. 77, Astronomical Data Analysis Software and Systems IV, R. A. Shaw, H. E. Payne, & J. J. E. Hayes, ed., pp. 349–+

Kundu A., Whitmore B. C., 2001a, AJ, 121, 2950

—, 2001b, AJ, 122, 1251

Kuntschner H., 2004, A&A, 426, 737

Kuntschner H., Emsellem E., Bacon R., Bureau M., Cappellari M., Davies R. L., de Zeeuw P. T., Falcón-Barroso J., Krajnović D., McDermid R. M., Peletier R. F., Sarzi M., 2006, MNRAS, 369, 497

Kuntschner H., Emsellem E., Bacon R., Cappellari M., Davies R. L., de Zeeuw P. T., Falcón-Barroso J., Krajnović D., McDermid R. M., Peletier R. F., Sarzi M., Shapiro K. L., van den Bosch R. C. E., van de Ven G., 2010, MNRAS, 408, 97

Landolt A. U., 2009, AJ, 137, 4186

Larsen S. S., Brodie J. P., 2002, AJ, 123, 1488

Larsen S. S., Brodie J. P., Beasley M. A., Forbes D. A., 2002, AJ, 124, 828

Lotz J. M., Miller B. W., Ferguson H. C., 2004, ApJ, 613, 262

Mackey A. D., van den Bergh S., 2005, MNRAS, 360, 631

Mackey D., Huxor A., Ferguson A., Irwin M., Tanvir N., McConnachie A., Ibata R., Chapman S., Lewis G., 2010, ArXiv e-prints

Madrid J. P., Graham A. W., Harris W. E., Goudfrooij P., Forbes D. A., Carter D., Blakeslee J. P., Spitler L. R., Ferguson H. C., 2010, ArXiv e-prints

Malin D., Hadley B., 1997, Publications of the Astronomical Society of Australia, 14, 52

Maraston C., 2005, MNRAS, 362, 799

Maraston C., Bastian N., Saglia R. P., Kissler-Patig M., Schweizer F., Goudfrooij P., 2004, A&A, 416, 467

McLaughlin D. E., van der Marel R. P., 2005, ApJS, 161, 304

Meylan G., Sarajedini A., Jablonka P., Djorgovski S. G., Bridges T., Rich R. M., 2001, AJ, 122, 830

Mieske S., Dabringhausen J., Kroupa P., Hilker M., Baumgardt H., 2008a, Astronomische Nachrichten, 329, 964

Mieske S., Hilker M., Infante L., 2002, A&A, 383, 823

—, 2004, A&A, 418, 445

Mieske S., Hilker M., Infante L., Jordán A., 2006a, AJ, 131, 2442

Mieske S., Hilker M., Jordán A., Infante L., Kissler-Patig M., Rejkuba M., Richtler T., Côté P., Baumgardt H., West M. J., Ferrarese L., Peng E. W., 2008b, A&A, 487, 921

Mieske S., Hilker M., Misgeld I., Jordán A., Infante L., Kissler-Patig M., 2009, A&A, 498, 705

Mieske S., Jordán A., Côté P., Kissler-Patig M., Peng E. W., Ferrarese L., Blakeslee J. P., Mei S., Merritt D., Tonry J. L., West M. J., 2006b, ApJ, 653, 193

Mieske S., Jordan A., Cote P., Peng E., Ferrarese L., Blakeslee J., Mei S., Baumgardt H., Tonry J., Infante L., West M., 2010, ArXiv e-prints

Misgeld I., Mieske S., Hilker M., 2008, A&A, 486, 697

Murray N., 2009, ApJ, 691, 946

Norris M. A., Sharples R. M., Bridges T., Gebhardt K., Forbes D. A., Proctor R., Raul Faifer F., Carlos Forte J., Beasley M. A., Zepf S. E., Hanes D. A., 2008, MNRAS,

385, 40

Norris M. A., Sharples R. M., Kuntschner H., 2006, MN-RAS, 367, 815

Paudel S., Lisker T., Janz J., 2010a, ArXiv e-prints

Paudel S., Lisker T., Kuntschner H., Grebel E. K., Glatt K., 2010b, MNRAS, 405, 800

Peacock M. B., Maccarone T. J., Waters C. Z., Kundu A., Zepf S. E., Knigge C., Zurek D. R., 2009, MNRAS, 392, L55

Peng C. Y., Ho L. C., Impey C. D., Rix H.-W., 2002, AJ, 124, 266

Peng E. W., Jordán A., Blakeslee J. P., Mieske S., Côté P., Ferrarese L., Harris W. E., Madrid J. P., Meurer G. R., 2009, ApJ, 703, 42

Peng E. W., Jordán A., Côté P., Blakeslee J. P., Ferrarese L., Mei S., West M. J., Merritt D., Milosavljević M., Tonry J. L., 2006, ApJ, 639, 95

Phillipps S., Drinkwater M. J., Gregg M. D., Jones J. B., 2001, ApJ, 560, 201

Price J., Phillipps S., Huxor A., Trentham N., Ferguson H. C., Marzke R. O., Hornschemeier A., Goudfrooij P., Hammer D., Tully R. B., Chiboucas K., Smith R. J., Carter D., Merritt D., Balcells M., Erwin P., Puzia T. H., 2009, MNRAS, 397, 1816

Proctor R. N., Forbes D. A., Beasley M. A., 2004, MNRAS, 355, 1327

Puzia T. H., Kissler-Patig M., Thomas D., Maraston C., Saglia R. P., Bender R., Goudfrooij P., Hempel M., 2005, A&A, 439, 997

Rejkuba M., Dubath P., Minniti D., Meylan G., 2007, A&A, 469, 147

Rhode K. L., Zepf S. E., 2004, AJ, 127, 302

Robin A. C., Reylé C., Derrière S., Picaud S., 2003, A&A, 409, 523

Sage L. J., Galletta G., 1994, AJ, 108, 1633

Sánchez-Blázquez P., Gorgas J., Cardiel N., González J. J., 2006, A&A, 457, 809

Sarzi M., Falcón-Barroso J., Davies R. L., Bacon R., Bureau M., Cappellari M., de Zeeuw P. T., Emsellem E., Fathi K., Krajnović D., Kuntschner H., McDermid R. M., Peletier R. F., 2006, MNRAS, 366, 1151

Schlegel D. J., Finkbeiner D. P., Davis M., 1998, ApJ, 500, 525

Sersic J. L., 1968, Atlas de galaxias australes. Cordoba

Sikkema G., Peletier R. F., Carter D., Valentijn E. A., Balcells M., 2006, A&A, 458, 53

Sirianni M., Jee M. J., Benítez N., Blakeslee J. P., Martel A. R., Meurer G., Clampin M., De Marchi G., Ford H. C., Gilliland R., Hartig G. F., Illingworth G. D., Mack J., McCann W. J., 2005, PASP, 117, 1049

Skrutskie M. F., Cutri R. M., Stiening R., et al.,, 2006, AJ, 131, 1163

Spitler L. R., Larsen S. S., Strader J., Brodie J. P., Forbes D. A., Beasley M. A., 2006, AJ, 132, 1593

Strader J., Brodie J. P., Spitler L., Beasley M. A., 2006, AJ, 132, 2333

Tamura N., Sharples R. M., Arimoto N., Onodera M., Ohta K., Yamada Y., 2006, MNRAS, 373, 601

Taylor M. A., Puzia T. H., Harris G. L., Harris W. E., Kissler-Patig M., Hilker M., 2010, ApJ, 712, 1191

Thomas D., Maraston C., Bender R., 2003, MNRAS, 339, 897

Thomas D., Maraston C., Korn A., 2004, MNRAS, 351, L19

Tonry J. L., Dressler A., Blakeslee J. P., Ajhar E. A., Fletcher A. B., Luppino G. A., Metzger M. R., Moore C. B., 2001, ApJ, 546, 681

Trager S. C., Worthey G., Faber S. M., Burstein D., Gonzalez J. J., 1998, ApJS, 116, 1

Vazdekis A., Sánchez-Blázquez P., Falcón-Barroso J., Cenarro A. J., Beasley M. A., Cardiel N., Gorgas J., Peletier R. F., 2010, MNRAS, 404, 1639

Wehner E. M. H., Harris W. E., 2007, ApJ, 668, L35

Wei L. H., Kannappan S. J., Vogel S. N., Baker A. J., 2010, ApJ, 708, 841

APPENDIX A: INVESTIGATION OF THE NGC3923 BLUE TILT

A closer look at Figure 8 indicates the possible presence of a "blue tilt" (Harris et al. 2006; Mieske et al. 2006b; Strader et al. 2006) in the blue GC population. The blue tilt appears to be a common feature of the GC systems of massive galaxies and is usually interpreted as being the result of a mass-metallicity relation due to more massive GCs being able to self-enrich more than their lower mass counterparts.

To determine the significance of the NGC3923 blue tilt we follow a procedure similar to that used by most other studies of this phenomenon (e.g. Peng et al. 2009, for M87 GCs). We limit our sample to GCs with $M_I < -8.34$, ensuring that we work only with objects with acceptable photometric errors. The effect of this limit is likely to be negligible, as the blue tilt is found to be driven by GCs more luminous than $M_I \sim -10$ (Harris 2009; Peng et al. 2009). We next bin our GCs by magnitude into four bins of approximately equal numbers of GCs (N > 100 in each). We fit the peak positions of the blue and red GC distributions of each bin using the KMM method (Ashman et al. 1994b), with errors in the measured colours of the red and blue peaks determined from 50 Monte-Carlo resimulations of the data within the photometric noise. We then fit a simple linear relation to the positions of the red and blue peaks. This is likely to be a significant simplification as the blue tilt is expected to display a curve at higher luminosities (see Harris 2009). However with the limited statistics available for this sample a first order model is all that can be reliably fit.

The best-fit slopes $\gamma_I = \frac{d(V-I)}{dI}$ to the peak colours of the blue and red populations are $\gamma_{I,\text{blue}} = -0.024 \pm 0.007$ and $\gamma_{I,\text{red}} = +0.012 \pm 0.013$ respectively. We therefore detect a blue tilt at greater than 3σ significance. However, in common with other studies we find no compelling evidence for a corresponding trend in the red GCs of NGC3923. Our measured slopes are indistinguishable from those measured by Peng et al. (2009) for the GCs of M87 ($\gamma_{I,\text{blue}} = -0.024 \pm 0.006$ and $\gamma_{I,\text{red}} = +0.003 \pm 0.007$).

APPENDIX B: INVESTIGATION OF THE NGC3923 GCLF

Figure 12 shows the results of our examination of the GCLF of NGC3923. In this analysis we have made use of the pho-

tometry of all GCs examined in Sections 2.6.1 and 2.6.3 with V < 24.75, ensuring we are operating within the region where incompleteness is negligible (the I band 90% and 50% completeness limits are 24.3 and 24.6 respectively). We remove contamination following the methods of Sikkema et al. (2006). To statistically remove foreground stars we make use of the Besancon model for the distribution of Milky Way stars (Robin et al. 2003). Unresolved background galaxies were removed statistically by applying our GC selection criteria to observations of the Hubble Deep Field South.

We bin the resulting V-band GC photometry and fit a single Gaussian to the observed histogram. As shown in Figure 12 the resulting turnover magnitude is entirely consistent with the observed universal GCLF turnover magnitude of $\sim -7.4 \pm 0.1$ (e.g. Kundu & Whitmore 2001a,b; Jordán et al. 2007) for the assumed distance of NGC3923. The GCLF analysis therefore provides independent verification of the assumed distance modulus of NGC3923. The measured 1.27 mag GCLF dispersion of the NGC3923 GCLF is also consistent with values found for other massive ellipticals (see e.g. Hilker 2009a).